DIFFERENTIAL DISTORTIONS IN PHOTOGRAMMETRIC BLOCK ADJUSTMENT

AUSTIN JOSEPH PUK NEE VOON

February 1986

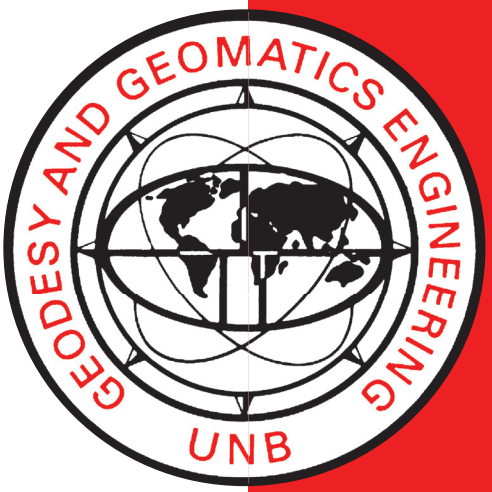

TECHNICAL REPORT
NO. 123

PREFACE

In order to make our extensive series of technical reports more readily available, we have scanned the old master copies and produced electronic versions in Portable Document Format. The quality of the images varies depending on the quality of the originals. The images have not been converted to searchable text.

DIFFERENTIAL DISTORTIONS IN PHOTOGRAMMETRIC BUNDLE BLOCK ADJUSTMENT

Austin Joseph Puk Nee Voon

Department of Geodesy and Geomatics Engineering
University of New Brunswick
P.O. Box 4400
Fredericton, N.B.
Canada
E3B 5A3

February 1986
Latest Reprinting February 1994

ABSTRACT

The self-calibrating photogrammetric bundle-block adjustment program UNBASC2 is revised. Its design matrices are rederived to account for the additional parameters being a function of the radial distance of image points. The revision improved the adjusted image coordinates by up to two micrometres. Similar revisions were made to the program GEBAT.

With improved mathematical modelling, further differential increase in the precision of photogrammetric densification may be achieved by improving the weighting scheme. Ignoring correlation in the weight matrices of observations and known parameters can lead to differential distortions.

Weights for observed image coordinates and for known coordinates of ground control points are examined. It is shown that in the presence of additional parameters, image weights transformed from the observation space to the model space will always be correlated. A test adjustment shows the maximum correlation to be 2.5%, resulting in changes to the adjusted coordinates of not more than 0.5 micrometres.

A similar improvement is obtained with the proper weighting of the ground control points in UNBASC2.

Although many bundle adjustment programs can treat ground control points as stochastic, they are not designed to accept their full covariance matrix even though there can be very high correlations. Evidence of highly correlated covariance matrices of the adjusted coordinates from weighted station adjustments of control networks are presented. It is shown that similar high correlation patterns can also occur in photogrammetric densification adjustments.

The implications of the high correlation on geodetic densification are illustrated by the global ripple effects and the importance of relative precision. Alternative apriori covariance matrices are proposed. Although these are not suitable for rigorous statistical assessment, they produce coordinates with acceptable distortions.

When a matrix inverse is involved, the effects of a distortion on the least squares solution may not be readily apparent. Therefore, the method of differential distortion analysis is developed to clarify the effects of each distorting variable.

TABLE OF CONTENTS

LIST OF TABLES

LIST OF ILLUSTRATIONS

ACKNOWLEDGEMENTS

I wish to thank Dr Wolfgang Faig, my supervisor, and John Porter for their advice, encouragement and support; Winnie and Frederick for their understanding and patience; Dr Hideya Moniwa, Dr Sabri El-Hakim, Dr Robin Steeves, and Michael Chapman for their assistance and the use of their programs; Allen Flemming, Urbain Arsenault, Bert Seely and Robert Craig for assistance with research data; Phil Mackenzie for his critical review; Byron Glass for his careful reading and the Land Registration and Information Service, as well as the Alberta Bureau of Surveying and Mapping for the use of their computing facilities.

DEDICATION

To my parents

CHAPTER I

INTRODUCTION

Photogrammetric bundle block adjustment development concentrated originally on the computational aspects rather than on the stochastic modelling (Ackermann, 1981). A typical example is the solution of the large systems of equations using the Cholesky block factorization as developed for PATM-43 (Meixner, 1972) and implemented in UNBASC2 (Moniwa, 1977). There are many other programs with specialized data structures to take advantage of the sparseness of the normal equation matrix. Although these computational aspects are not dealt with in detail here, some consequences of these specializations are briefly discussed in section 7.1.

Recent and current efforts in bundle adjustment are

directed at improving the mathematical model. Of special interests are the use of additional parameters to model residual systematic errors, the consideration of correlated observations and the treatment of ground control points as non-stochastic.

Additional parameters used by different researchers seem to vary widely. Kilpela (1980) summarizes fourteen parameter sets that were being studied empirically. Investigations into two parameter sets, in use at the University of New Brunswick, resulted in revisions to their implemented design matrices. Revisions to the design matrices of UNBASC2 are presented in chapter III and of GEBAT-D in chapter IV. The differential distortions resulting from the original UNBASC2 design matrices are also presented.

Correlation of image coordinates have been estimated by Forstner and Schroth (1981). Schroth (1984) and Jacobsen (1984) further extended the study to include correlation between images. Ligterink (1984) and Voorden (1984) analyzed the influence of correlated observations on internal reliability of photogrammetric (independent model) blocks. However, correlations arising from the weight propagation of image coordinates to account for additional

parameters have not been addressed. Chapter 3 discusses such a propagation, its validity and the differential changes it caused in the solution.

Photogrammetric bundle block adjustments have often been proposed as a viable alternative to traditional geodetic adjustments for control densification. For example, Brown (1977) demonstrated that with the use of bundle adjustments with self-calibration, the benefit-to-cost ratio of densification may be doubled.

However, integration of the photogrammetric densification and the geodetic networks can be more acceptable if the contemporary treatment of ground control points as non-correlated is reconsidered. For coordinates obtained from photogrammetric adjustments to be acceptable in the densification of geodetic networks, they must be of sufficient precision. Furthermore, the densification should result in a well integrated network that is compatible with the existing geodetic control points. Precision has been shown to be adequate for densification, as demonstrated in the Sudbury test area where a planimetric precision of two centimetres has been obtained at a photo scale of 1:4400 (El-Hakim, 1982).

The compatibility of the photogrammetric and the geodetic coordinates has been more problematic. This is in part due to the traditional relative precision specifications of geodetic networks (EMR, 1978) versus the global absolute precision quoted for photogrammetric block adjustments. In fact, it was not until recently that error ellipses (Jacobsen, 1980) and ellipsoids (El-Hakim, 1982) have been presented in photogrammetric results. Lucas (1978) stated the requirement for standard deviations of the distance and azimuth between all pairs of intervisible ground points.

Another reason the compatibility issue has not been dealt with in as much detail as the precision issue is the general lack of the covariance matrices of both the geodetic and photogrammetric coordinates. The first significant covariance matrix of a second order geodetic network became available in Canada only in 1979 as a result of the ATS77 redefinition and readjustment of the LRIS network in the Maritimes (Nickerson, 1981). The full covariance matrix for the North American Datum 1983 is expected to be available (Hanson, 1978) upon completion of that readjustment. Bundle adjustment programs such as BOBUE (Kupfer & Mauelshagen, 1980) Gentri (Larsson, 1984)

and BMAC (Chapman, 1985) are capable of producing the full covariance matrix. However, production systems in Canada generally use independent model block adjustment programs like PATM-43 and SPACE-M which do not have such capability.

Current bundle adjustment programs make certain assumptions with regards to weighting ground control points. It is generally possible to choose different weight matrices for groups of points. However, covariance information between the ground control points is still ignored to avoid destroying the sparseness of the normal equation matrix. Unfortunately, as pointed out by Molenaar (1984) "the structure of land surveying networks gives correlation among coordinates".

Such high correlations will be illustrated in chapter 5 with case studies of actual production projects where the variance-covariance matrices of geodetic control points are available. The high correlations have important ramifications for photogrammetric (and other) control densification.

Firstly, the photogrammetric densification adjustment should be reviewed to see if it does not itself create such

high correlations. Faig (1973) and Grun (1978) reported some high correlations amongst the interior orientation parameters while (Kupfer & Mauelshagen, 1980) showed that they may even exist for other parameters. To demonstrate a potential cause of highly correlated covariance matrices of the adjusted parameters, an experimental densification is simulated. Findings are presented in chapter 6.

Secondly, the traditional approaches to mathematical maintenance may no longer be valid when there is a highly correlated covariance matrix of the adjusted parameters. In section 7.1 it is shown that the 'ripple effects' may no longer be localized around the region of change.

Thirdly, the full precision of the ground control points is not considered when they are treated as independent. However, the cost of providing the covariance matrix can be very expensive. Therefore, alternatives to these matrices are explored in section 7.3.

Fourthly, neglecting the covariances may still produce acceptable coordinates but unsuitable covariances for rigorous statistical analyses. This is demonstrated in section 7.4

To analyze the ripple effects and to verify the numerical values of the above differential distortions, some simple analytical expressions are sought. Those of the sequential adjustment model (Nickerson, 1979 & Rosculet, 1980) were ruled out due to the difficulty in analysing the effects of each distorting component. An approach whereby components of distorting quantities may be analyzed individually, is proposed in chapter II.

CHAPTER II

METHOD OF DIFFERENTIAL DISTORTION ANALYSIS

Partial derivatives of matrices are used in linearizing systems of equations. Specifically, the mathematical function is differentiated with respect to the parameters and the observables, resulting in the design matrices (equations 2.17 & 2.18). However, in the context of analyzing differential distortions, it is the change in the solution due to changes in the coefficients and independent variables that are of interest. Faddeev and Faddeeva (1963) used this technique to define an ill-conditioned matrix which can lead to an unstable solution.

This technique is extended to analyze differential changes in the least squares adjustment.

2.1 Matrix Differentiation

The partial derivative of a matrix A with respect to one of its elements a_{ij} is denoted as:

$$\frac{\partial A}{\partial a} = \Delta_a \tag{2.1a}$$

where Δ is a matrix with the value 1 for the element ij involved and 0 elsewhere. If the matrix is symmetric, the transposed element ji is also 1.

Alternatively, eq. (2.1a) may be expressed as

$$\partial A = \Delta_a \partial a = \Delta_{\partial a} \tag{2.1b}$$

where Δ_∂ is then a matrix of ∂ for the elements involved and 0 elsewhere.

2.1.1 Matrix Product

The partial derivative of the product of two matrices follows the same product rule as the derivative of scalar variables. An important distinction is that the order of the matrix multiplication must be preserved as shown below:

$$\frac{\partial AB}{\partial t} = \frac{\partial A}{\partial t} B + A \frac{\partial B}{\partial t} \tag{2.2}$$

2.1.2 Matrix Inverse

The most important property of the partial derivatives for distortion analysis of an adjustment is the partial derivative of an inverse:

$$\frac{\partial N^{-1}}{\partial t} = - N^{-1} \frac{\partial N}{\partial t} N^{-1} \qquad (2.3)$$

Various proofs are available in several texts such as Faddeev & Faddeeva (1963), Frazer & Collar (1965), Bronson (1970) and Wells (1971). Because of the crucial role this property plays in the development of the differential distortion equations, a short proof is given below.

Write, for the identity matrix I, $I = N^{-1}N$ (2.4)

Differentiating both sides and applying eq. (2.2),

$$\frac{\partial I}{\partial t} = \frac{\partial N^{-1}}{\partial t} N + N^{-1}\frac{\partial N}{\partial t}$$

That is,

$$0 = \frac{\partial N^{-1}}{\partial t} N + N^{-1}\frac{\partial N}{\partial t}$$

Therefore,

$$\frac{\partial N^{-1}}{\partial t} N = - N^{-1}\frac{\partial N}{\partial t}$$

Postmultiplying by N^{-1},

$$\frac{\partial N^{-1}}{\partial t} NN^{-1} = - N^{-1}\frac{\partial N}{\partial t} N^{-1}$$

Therefore,

$$\frac{\partial N^{-1}}{\partial t} = - N^{-1}\frac{\partial N}{\partial t} N^{-1}$$

(q.i.d.)

2.2 Least Squares Equations

The equations for the combined and the parametric cases with weighted parameters (Krakiwsky, 1975; Vanicek & Krakiwsky, 1982), are only listed here without proof. The parametric equations are a special case of the combined equations when B = -I (eq. 2.18b). Where the equations are not qualified, they apply to both the combined and the parametric cases.

Solution vector $\hat{x} = - N^{-1}u$ (2.5)

Final adjusted parameters $\hat{X} = X^o + \hat{x}$ (2.6)

Estimated residuals

Combined: $\hat{r} = - C_r B^T M(A\hat{x} + w)$ (2.7a)

Parametric: $\hat{r} = A\hat{x} + w$ (2.7b)

Adjusted observations $\hat{l} = l + \hat{r}$ (2.8)

Apriori variance factor (df degree of freedom) $\hat{\sigma}_o^2 = \dfrac{\hat{r}^T P_r \hat{r} + \hat{x}^T P_X \hat{x}}{df}$ (2.9)

Covariance matrix of $\hat{X}$ $C_{\hat{X}} = N^{-1} = C_{\hat{x}}$ (2.10)

Covariance matrix of $\hat{r}$

Combined: $C_{\hat{r}} = C_r B^T M(I - AC_{\hat{X}}A^T M)BC_r$ (2.11a)

Parametric: $C_{\hat{r}} = C_r - AC_{\hat{X}}A^T$ (2.11b)

Covariance matrix of $\hat{l}$ $C_{\hat{l}} = C_r - C_{\hat{r}}$ (2.12)

where Combined: $M = (BC_r B^T)^{-1}$ (2.13a)

Parametric: $M = C_r^{-1} = P_l$ (2.13b)

Normal equations $N = A^T M A + P_X$ (2.14)

Unknown vector $u = A^T M w + P_X w_X$ (2.15)

Misclosure vector $w = F(X^o, l)$ (2.16)

First design matrix $A = \frac{\partial F}{\partial X}\Big|_{X^o, l}$ (2.17)

Second design matrix

Combined: $B = \frac{\partial F}{\partial l}\Big|_{X^o, l}$ (2.18a)

Parametric: $B = - I$ (2.18b)

Observation weight matrix $P_l = C_l^{-1} = C_r^{-1} = P_r$ (2.19)

Parameter weight matrix $P_X = C_X^{-1} = ((C_X)_s)^{-1}$ (2.20)
(s being a subset)

2.3 Partial Derivatives of the Solution Vector

Among the partial derivatives of the least squares equations, the derivative of the solution vector is of primary interest. This is obtained by applying the method of partial derivatives of a matrix inverse (eq. 2.3) and the chain rule for matrix products (eq. 2.2) to the

solution vector (eq.2.5) as follows:

For $\hat{x} = - N^{-1}u$

$$\frac{\partial \hat{x}}{\partial t} = - \frac{\partial N^{-1}}{\partial t} u - N^{-1}\frac{\partial u}{\partial t}$$

$$= N^{-1}\frac{\partial N}{\partial t} N^{-1}u - N^{-1}\frac{\partial u}{\partial t}$$

Substituting equations (2.5 & 2.10),

$$\frac{\partial \hat{x}}{\partial t} = - C_{\hat{x}} \frac{\partial N}{\partial t} \hat{x} - C_{\hat{x}} \frac{\partial u}{\partial t} \qquad (2.21)$$

where the parameter t may be one of a, m, w, p_X or w_X, being elements of the components of equations (2.14 & 2.15).

2.3.1 Normal Equation Components

Using the notation of eq. (2.1a), the partial derivatives of the normal equations (eq. 2.14) are:

$$\frac{\partial N}{\partial a} = \frac{\partial A^T}{\partial a} MA + A^T\frac{\partial M}{\partial a} A + A^TM \frac{\partial A}{\partial a} + \frac{\partial P_X}{\partial a}$$

$$= \Delta_a^T MA + 0 + A^TM\Delta_a + 0 \qquad (2.22a)$$

$$\frac{\partial N}{\partial m} = \frac{\partial A^T}{\partial m} MA + A^T\frac{\partial M}{\partial m} A + A^TM \frac{\partial A}{\partial m} + \frac{\partial P_X}{\partial m}$$

$$= A^T\Delta_m A \qquad (2.22b)$$

$$\frac{\partial N}{\partial w} = 0 \qquad (2.22c)$$

$$\frac{\partial N}{\partial p_X} = \frac{\partial A^T}{\partial p_X} MA + A^T \frac{\partial M}{\partial p_X} A + A^T M \frac{\partial A}{\partial p_X} + \frac{\partial P_X}{\partial p_X}$$

$$= \Delta_{p_X} \qquad (2.22d)$$

$$\frac{\partial N}{\partial w_X} = 0 \qquad (2.22e)$$

2.3.2 Unknown Vector Components

Similarly, the partial derivatives of the unknown vector (eq. 2.15) are:

and $$\frac{\partial u}{\partial a} = \frac{\partial A^T}{\partial a} Mw + A^T \frac{\partial M}{\partial a} w + A^T M \frac{\partial w}{\partial a} + \frac{\partial P_X}{\partial a} w_X + P_X \frac{\partial w_X}{\partial a}$$

$$= \Delta_a^T Mw \qquad (2.23a)$$

$$\frac{\partial u}{\partial m} = A^T \Delta_m w \qquad (2.23b)$$

$$\frac{\partial u}{\partial w} = A^T M \Delta_w \qquad (2.23c)$$

$$\frac{\partial u}{\partial p_X} = \Delta_{p_X} w_X \qquad (2.23d)$$

$$\frac{\partial u}{\partial w_X} = P_X \Delta_{w_X} \qquad (2.23e)$$

2.4 Differential Distortions for the Paramteric Case

Equations of the differential distortions for the parameteric case are obtained by taking the partial derivatives of the solution vector (eq. 2.5), the estimated residuals (eq. 2.7b), their covariance matrices (equations 2.10 & 2.11a) and the aposteriori variance factor (eq.2.9) with respect to differential elements of the first design matrix, the observation and parameter weights and the misclosure vector. The derivation makes use of equations (2.21 to 2.23) as well as the following:

$$MC_{\hat{l}} = C_r^{-1}(C_r - C_{\hat{r}}) = I - MC_{\hat{r}} \tag{2.24}$$

$$MC_{\hat{r}}P_r\hat{r} = P_r\hat{r} \tag{2.25}$$

$$C_{\hat{X}}A^TP_r\hat{r} = 0 \tag{2.26}$$

2.4.1 First Design Matrix

Differential distortions due to ∂a, e.g. from changes in the geometric configuration of a network, are as follows:

$$\frac{\partial C_{\hat{X}}}{\partial a} = - C_{\hat{X}}A^TM\Delta_a C_{\hat{X}} - C_{\hat{X}}\Delta_a^TMAC_{\hat{X}} \tag{2.27a}$$

$$\frac{\partial \hat{x}}{\partial a} = - C_{\hat{X}}A^TM\Delta_a \hat{x} - C_{\hat{X}}\Delta_a^TM\hat{r} \tag{2.27b}$$

$$\frac{\partial C_{\hat{r}}}{\partial a} = - C_{\hat{r}} M \Delta_a C_{\hat{X}} A^T - A C_{\hat{X}} \Delta_a^T M C_{\hat{r}} \qquad (2.27c)$$

$$\frac{\partial \hat{r}}{\partial a} = C_{\hat{r}} M \Delta_a \hat{x} - A C_{\hat{X}} \Delta_a^T M \hat{r} \qquad (2.27d)$$

$$\frac{\partial \hat{\sigma}_o^2}{\partial a} = \frac{\hat{r}^T P_r \Delta_a \hat{x} - \hat{x}^T \Delta_a^T P_r \hat{r}}{df} \qquad (2.27e)$$

2.4.2 Observation Weight Matrix

Differential distortions due to ∂m, e.g. in neglecting the correlation of image coordinate observations, are as follows:

$$\frac{\partial C_{\hat{X}}}{\partial m} = - C_{\hat{X}} A^T \Delta_m A C_{\hat{X}} \qquad (2.28a)$$

$$\frac{\partial \hat{x}}{\partial m} = - C_{\hat{X}} A^T \Delta_m \hat{r} \qquad (2.28b)$$

$$\frac{\partial C_{\hat{r}}}{\partial m} = A C_{\hat{X}} A^T \Delta_m A C_{\hat{X}} A^T = C_{\hat{l}} \Delta_m C_{\hat{l}} \qquad (2.28c)$$

$$\frac{\partial \hat{r}}{\partial m} = - A C_{\hat{X}} A^T \Delta_m \hat{r} = - C_{\hat{l}} \Delta_m \hat{r} \qquad (2.28d)$$

$$\frac{\partial \hat{\sigma}_o^2}{\partial m} = \frac{\hat{r}^T \Delta_m \hat{r}}{df} \qquad (2.28e)$$

2.4.3 Parameter Weight Matrix

Differential distortions due to ∂p_X, e.g. in neglecting the correlation of ground control point coordinates, are as follows:

$$\frac{\partial C_{\hat{X}}}{\partial p_X} = - C_{\hat{X}} \Delta_{p_X} C_{\hat{X}} \tag{2.29a}$$

$$\frac{\partial \hat{x}}{\partial p_X} = - C_{\hat{X}} \Delta_{p_X} (\hat{x} + w_X) \tag{2.29b}$$

$$\frac{\partial C_{\hat{r}}}{\partial p_X} = A C_{\hat{X}} \Delta_{p_X} C_{\hat{X}} A^T \tag{2.29c}$$

$$\frac{\partial \hat{r}}{\partial p_X} = - A C_{\hat{X}} \Delta_{p_X} (\hat{x} + w_X) \tag{2.29d}$$

$$\frac{\partial \hat{\sigma}_o^2}{\partial p_X} = \frac{- (\hat{x}^T + w_X^T) \Delta_{p_X} C_{\hat{X}} P_X \hat{x} + \hat{x}^T \Delta_{p_X} \hat{x} - \hat{x}^T P_X C_{\hat{X}} \Delta_{p_X} (\hat{x} + w_X)}{df} \tag{2.29e}$$

2.4.4 Observations

Differential distortions due to $\partial l = - \partial w$, e.g. gross error in observations, are as follows:

$$\frac{\partial C_{\hat{X}}}{\partial w} = 0 \tag{2.30a}$$

$$\frac{\partial \hat{x}}{\partial w} = C_{\hat{X}} A^T M \Delta_w \tag{2.30b}$$

$$\frac{\partial C_{\hat{r}}}{\partial w} = 0 \qquad (2.30c)$$

$$\frac{\partial \hat{r}}{\partial w} = - C_{\hat{r}} M \Delta_w \qquad (2.30d)$$

$$\frac{d\hat{\sigma}_o^2}{\partial w} = - \frac{\hat{r}^T P_r \Delta_w + \Delta_w^T P_r \hat{r}}{df} \qquad (2.30e)$$

2.4.5 Parameter Observations

Differential distortions due to Δw_X are as follows:

$$\frac{\partial C_{\hat{X}}}{\partial w_X} = 0 \qquad (2.31a)$$

$$\frac{\partial \hat{x}}{\partial w_X} = - C_{\hat{X}} P_X \Delta_{w_X} \qquad (2.31b)$$

$$\frac{\partial C_{\hat{r}}}{\partial w_X} = 0 \qquad (2.31c)$$

$$\frac{\partial \hat{r}}{\partial w_X} = - A C_{\hat{X}} P_X \Delta_{w_X} \qquad (2.31d)$$

$$\frac{\partial \hat{\sigma}_o^2}{\partial w_X} = - \frac{\hat{x}^T P_X C_{\hat{X}} P_X \Delta_{w_X} + \Delta_{w_X}^T P_X C_{\hat{X}} P_X \hat{x}}{df} \qquad (2.31e)$$

2.5 Comparison With Other Methods

Several methods dealing with incremental or

differential changes are briefly compared with the method of differential distortion analysis developed in this chapter.

2.5.1 Sequential Adjustment

The sequential method provides an efficient means of updating the solution vector and its covariance matrix when parameters or observations are either being added to or deleted from the adjustment. Using subscripts 1 and 2 to denote the matrices before and after the changes, the sequential expressions (Nickerson, 1979) are:

$$\hat{x}_2 = \hat{x}_1 - C_{\hat{X}_1} A_2^T (\pm M_2 + A_2 C_{\hat{X}_1} A_2^T)^{-1} (A_2 \hat{x}_1 + w_2) \qquad (2.32)$$

$$C_{\hat{X}_2} = C_{\hat{X}_1} - C_{\hat{X}_1} A_2^T (\pm M_2 + A_2 C_{\hat{X}_1} A_2^T)^{-1} A_2 C_{\hat{X}_1} \qquad (2.33)$$

The differential distortion analysis method does not handle changes in the number of parameters but the sequential method does. However, the sequential method has two major disadvantages. One disadvantage is, that the expressions still contain a new inverse so that it is as cumbersome as the original least squares expression. The other is, that components of the distortions are not separated in the manner shown in chapter 2.4.

2.5.2 Strain Analysis

Eq. (2.30d) is used as the basis of strain analysis by Dare and Vanicek (1982). They expressed $\nabla\hat{x}$ as the displacement response due to $\Delta_{\nabla 1}$.

2.5.3 Data Snooping

With Baarda's data snooping, the effect of the gross error ∇l on the residuals is given by the eq. (2.30d). Diagonal elements of $C_{\hat{r}}M$ are the redunancy numbers (El-Hakim, 1981) that indicate the reliability of each observation. It is noted that these redundancy numbers also appear in equations (2.27c & d).

2.5.4 Global Roundoff Error Analysis

Meissl (1978) used Wilkinson's method of tracing errors backwards (instead of propagating them forward) to predict global roundoff errors in solving the perturbed NAD83 normal equations as follows:

$$\nabla\hat{x} = - C_{\hat{X}}\Delta_{\nabla n}\hat{x} \qquad (2.34)$$

The same linear approximation can be obtained with the method of differential distortion analysis. This is done by setting t=n in eq. (2.21) and using the notation of eq.

(2.1b).

2.5.5 Rigorous Updating

To rigorously update a network, Cramer et al (1985) proposed some expressions derived with the matrix lemmas:

$$(C^{-1} + A^TB^{-1}A)^{-1} = C - CA^T(B + ACA^T)^{-1}AC \qquad (2.35)$$

and $$(C^{-1} + A^TB^{-1}A)^{-1}A^TB^{-1} = CA^T(B + ACA^T)^{-1} \qquad (2.36)$$

for an arbitary A and positive definite B and C (equations 3.22 & 3.23 of Vanicek & Krakiwsky, 1982). By substituting eq. (2.36) into eq. (2.35) and taking $C = N^{-1}$ and $\Delta_n = A^TB^{-1}A$, the expression

$$(N + \Delta_n)^{-1} = N^{-1} - (N + \Delta_n)^{-1}\Delta_nN^{-1} \qquad (2.37)$$

is obtained. By approximating $(N + \Delta_n)^{-1} \doteq N^{-1}$ on the right hand side, eq. (2.37) becomes

$$(N + \Delta_n)^{-1} \doteq N^{-1} - N^{-1}\Delta_nN^{-1} \doteq N^{-1}(I - \Delta_nN^{-1}) \qquad (2.38)$$

The same result is obtained with the method of differential distortion analysis, by setting t=n in eq. (2.3). To avoid the first order approximation in eq. (2.38), further rearrangement of eq. (2.37) gives the rigorous update of the inverse of the normal equations:

$$(N + \Delta_n)^{-1} = N^{-1}(I + \Delta_nN)^{-1} \qquad (2.39)$$

which again has the disadvantage of a new inversion.

CHAPTER III

DIFFERENTIAL DISTORTIONS IN UNBASC2

UNBASC2 (Moniwa, 1977) is a bundle block adjustment program with photo-variant self-calibration. Bundle adjustment is a fully analytical approach to photogrammetric triangulation. It is basically expressed by the collinearity equations. Assuming a distortion free central projection, the collinearity equations relate an object point, its image and the perspective center.

To account for systematic distortions in the central projection, additional parameters are introduced. Two methods of choosing the parameters, reduction and generalization, have been used. In the reduction method, the causes of the distortions are reduced to physical phenomena. Parameters suitable for compensating for these

physically explained distortions are added to the unknowns of the system. This is the method adopted in UNBASC2.

In the generalization method, the causes of the distortions are not distinguished. Rather, the generalized effects of these distortions are modelled and corrected for. GEBAT (see chapter 4) makes use of this method.

With self-calibration, the additional parameters are solved for along with the other unknowns. The same observations are used without relying on external information such as known coordinates of a test field.

If the parameters can be introduced for each photograph, as opposed to the whole block, the approach is termed photo-variant.

3.1 Collinearity Equations

For an ideal central projection,

$$\begin{bmatrix} x - x_o \\ y - y_o \\ -c \end{bmatrix} = \lambda\, R(\omega,\phi,\kappa) \begin{bmatrix} X - X_C \\ Y - Y_C \\ Z - Z_C \end{bmatrix} = \begin{bmatrix} M_1 \\ M_2 \\ M_3 \end{bmatrix} \qquad (3.1)$$

relates the unknown exterior orientation parameters (ω, ϕ, κ, X_C, Y_C, Z_C) to the object coordinates (X, Y, Z) via the scale λ and the rotation matrix R. Denoting cosine by C and sine by S

$$R = \begin{bmatrix} C\phi C\kappa, & C\omega S\kappa + S\omega S\phi C\kappa, & S\omega S\kappa - S\phi C\kappa C\omega \\ -C\phi S\kappa, & C\omega C\kappa - S\phi S\omega S\kappa, & S\omega C\kappa + S\phi S\kappa C\omega \\ S\phi, & -S\omega C\phi, & C\omega C\phi \end{bmatrix} \qquad (3.2)$$

The collinearity equations may then be expressed as:

$$x - x_o = - c \frac{M_1}{M_3} \qquad (3.3a)$$

$$y - y_o = - c \frac{M_2}{M_3} \qquad (3.3b)$$

for the observed image coordinates (x, y), the principal point (x_o, y_o) and the principal distance c.

3.2 UNBASC2 Mathematical Model

The UNBASC2 mathematical model is the implicit form of the standard combined case least squares adjustment. Two functional models, photogrammetric and geodetic, are combined.

3.2.1 UNBASC2 Functional Models

The photogrammetric model is the collinearity equations (equations 3.3) modified for additional parameters to account for systemmatic distortions:

$$F_x = ((x - x_o) + D_x) + c\,\frac{M_1}{M_3} = 0 \qquad (3.4a)$$

$$F_y = ((y - y_o) + D_y) + c\,\frac{M_2}{M_3} = 0 \qquad (3.4b)$$

where the distortion components are

$$D_x = (x - x_o)(k_1r^2 + k_2r^4 + k_3r^6) + p_1(r^2 + 2(x - x_o)^2) + 2p_2(x - x_o)(y - y_o) + A(y - y_o) \qquad (3.5a)$$

$$D_y = (y - y_o)(k_1r^2 + k_2r^4 + k_3r^6) + p_2(r^2 + 2(y - y_o)^2) + 2p_1(x - x_o)(y - y_o) + B(y - y_o) \qquad (3.5b)$$

for the radial distance

$$r = ((x - x_o)^2 + (y - y_o)^2)^{0.5} \qquad (3.6)$$

and the radial lens distortion (k_1, k_2, k_3), decentering lens distortion (p_1, p_2) and affinity of the image coordinates (A, B). Providing object space control is the goedetic model:

$$F_g = \begin{bmatrix} X_g - X \\ Y_g - Y \\ Z_g - Z \end{bmatrix} = 0 \qquad (3.7)$$

for ground control points (X_g, Y_g, Z_g).

3.2.2 UNBASC2 System of Normal Equations

With subscript p referring to the photogrammetric and g referring to the geodetic, the functional models of UNBASC2 (equations 3.4 & 3.7) are written implicitly as:

$$F_p(X_1, X_2, l_p) = 0 \qquad (3.8)$$

$$F_g(X_2, l_g) = 0 \qquad (3.9)$$

where X_1 is the vector of photo orientation elements and calibration parameters (x_o, y_o, c, X_C, Y_C, Z_C, ω, ϕ, κ, k_1, k_2, k_3, p_1, p_2, A, B)

X_2 is the vector of unknown object coordinates (X, Y, Z)

l_p is the vector of observed image coordinates (x, y) and

l_g is the vector of ground control coordinates (X_g, Y_g, Z_g).

The linearized differential forms of equations (3.8 & 3.9) are respectively

$$A_1\hat{X}_1 + A_2\hat{X}_2 + B_p\hat{r}_p + w_p = 0 \qquad (3.10)$$

$$A_2\hat{X}_2 + B_g\hat{r}_g + w_g = 0 \qquad (3.11)$$

where $\hat{x}_1$ and $\hat{x}_2$ are corrections to $\hat{X}_1$ and $\hat{X}_2$, the least squares estimates of X_1 and X_2 respectively

$\hat{r}_p$ and $\hat{r}_g$ are observation residuals

w_p and w_g are misclosure vectors

$$w_p = F_p(X_1^o,\ X_2^o,\ l_p) \tag{3.12}$$

$$w_g = F_g(X_2^o,\ l_g) \tag{3.13}$$

A_1, A_2, B_p, A_g, B_g are design matrices expressed, with superscript ^{o} as initial values:

$$A_1 = \frac{\partial F_p}{\partial X_1}\Bigg|_{X_1^o,\ X_2^o\ \ l_p} \tag{3.14}$$

$$A_2 = \frac{\partial F_p}{\partial X_2}\Bigg|_{X_1^o,\ X_2^o,\ l_p} \tag{3.15}$$

$$B_p = \frac{\partial F_p}{\partial l_p}\Bigg|_{X_1^o,\ X_2^o,\ l_p} \tag{3.16}$$

$$A_g = \frac{\partial F_g}{\partial X_2}\Bigg|_{X_2^o,\ l_g} \tag{3.17}$$

$$B_g = \frac{\partial F_g}{\partial l_g}\Bigg|_{X_2^o,\ l_g} \tag{3.18}$$

Applying the least squares principle of combining models, the variation function is written with a quadratic form for each set of observations and a constraint function for each of the models as

$$\phi = \hat{r}_p^T C_{r_p}^{-1} \hat{r}_p + 2\hat{k}_p^T (A_1 \hat{x}_1 + A_2 \hat{x}_2 + B_p \hat{r}_p + w_p)$$

$$+ \hat{r}_g^T C_{r_g}^{-1} \hat{r}_g + 2\hat{k}_g^T (A_2 \hat{x}_2 + B_g \hat{r}_g + w_g) \qquad (3.19)$$

where C_{r_p} and C_{r_g} are the covariance matrices of the photogrammetric and geodetic observations respectively,

$\hat{k}_p$ and $\hat{k}_g$ are the estimators for the vectors of Lagrange multipliers.

Taking the partial derivatives of (3.19) and setting each to be zero to obtain the minimum, the least squares equations are written as:

$$0 = \frac{\partial \phi}{\partial \hat{r}_p} = C_{r_p}^{-1} \hat{r}_p + B_p^T \hat{k}_p \qquad (3.20)$$

$$0 = \frac{\partial \phi}{\partial \hat{r}_g} = C_{r_g}^{-1} \hat{r}_g + B_p^T \hat{k}_p \qquad (3.21)$$

$$0 = \frac{\partial \phi}{\partial \hat{x}_1} = A_1^T \hat{k}_p \qquad (3.22)$$

$$0 = \frac{\partial \phi}{\partial \hat{x}_2} = A_2^T \hat{k}_p + A_g^T \hat{k}_g \qquad (3.23)$$

Writing equations (3.10, 3.11 & 3.20 to 3.23) in their most expanded form,

$$\begin{bmatrix} C_{r_p}^{-1} & B_p^T & 0 & 0 & 0 & 0 \\ B_p & 0 & 0 & 0 & A_1 & A_2 \\ 0 & 0 & C_{r_g}^{-1} & B_g^T & 0 & 0 \\ 0 & 0 & B_g & 0 & 0 & A_g \\ 0 & A_1^T & 0 & 0 & 0 & 0 \\ 0 & A_2^T & 0 & A_g^T & 0 & 0 \end{bmatrix} \begin{bmatrix} \hat{r}_p \\ \hat{k}_p \\ \hat{r}_g \\ \hat{k}_g \\ \hat{x}_1 \\ \hat{x}_2 \end{bmatrix} + \begin{bmatrix} 0 \\ w_p \\ 0 \\ w_g \\ 0 \\ 0 \end{bmatrix} = 0 \qquad (3.24)$$

Eliminating $\hat{r}_p$, $\hat{k_p}$, $\hat{r}_g$ and $\hat{k}_g$ by partitioning eq. (3.24) as

$$\begin{bmatrix} A & B \\ C & D \end{bmatrix} \begin{bmatrix} x \\ y \end{bmatrix} + \begin{bmatrix} E \\ F \end{bmatrix} = 0 \qquad (3.25)$$

and using the relationship (Krakiwsky, 1975)

$$(D - CA^{-1}B)y + (F - CA^{-1}E) = 0 \qquad (3.26)$$

successively, the normal equation system is obtained as

$$\begin{bmatrix} A_1^T M_p A_1 & A_1^T M_p A_2 \\ A_2^T M_p A_1 & A_2^T M_p A_2 + A_g^T M_g A_g \end{bmatrix} \begin{bmatrix} \hat{x}_1 \\ \hat{x}_2 \end{bmatrix} + \begin{bmatrix} A_1^T M_p w_p \\ A_2^T M_p w_p + A_g^T M_g w_g \end{bmatrix} = 0 \qquad (3.27)$$

where $M_p = (B_p C_{r_p} B_p^T)^{-1}$ (3.28)

$M_g = (B_g C_{r_g} B_g^T)^{-1} = C_{r_g}^{-1}$ (3.29)

since $A_g = -I$ and $B_g = I$, (3.30)

from equations (3.17, 3.18) of the geodetic model (eq. 3.7).

3.3 Image Weights

Eq. (3.28) transforms weights from the observation space to the model space (Vanicek & Krakiwsky, 1982). In the presence of additional parameters that are a function of the image coordinates, their weights M in the model space will always be correlated. As shown below, this is true even when the weight matrix, P, in the observation space is unity.

3.3.1 Weight Transformation to Model Space

Let $P_l = I$ (unit matrix). Hence

$$C_r = I = C_l. \tag{3.31}$$

For each image point, assuming no correlations between points, the second design matrix is

$$B = \begin{bmatrix} b_{11} & b_{12} \\ b_{21} & b_{22} \end{bmatrix} = \begin{bmatrix} \frac{\partial F_{p_x}}{\partial x} & \frac{\partial F_{p_y}}{\partial x} \\ \frac{\partial F_{p_x}}{\partial y} & \frac{\partial F_{p_y}}{\partial y} \end{bmatrix} \tag{3.32}$$

Substituting equations (3.31 & 3.32) into eq. (3.28), the transformed weight matrix of the observed image coordinates is

$$M = \begin{bmatrix} b_{11}^2 + b_{21}^2 & b_{11}b_{12} + b_{21}b_{22} \\ b_{11}b_{12} + b_{21}b_{22} & b_{12}^2 + b_{22}^2 \end{bmatrix}^{-1} \quad (3.33a)$$

$$= \begin{bmatrix} b_{12}^2 + b_{22}^2 & b_{21}b_{22} - b_{11}b_{12} \\ b_{21}b_{22} - b_{11}b_{12} & b_{11}^2 + b_{21}^2 \end{bmatrix} d^{-1} \quad (3.33b)$$

where $d = (b_{11}b_{22} - b_{21}b_{12})^2$ (3.34)

3.3.2 Image Correlation

To obtain an idea of the amount of x/y correlation, test data for the Edmunston block (Moniwa, 1977) was adjusted with unit weights and additional parameters. In the presence of additional parameters it can be shown, by inspecting equations (3.37a to d), that $B \neq I$. Thus, from eq. (3.33b), $M \neq I$.

For the 236 points, the maximum correlation was only 2.5%. Their mean was -0.0005% and their root mean square error was 0.36%. The mean being insignificantly different from zero may possibly be explained by (1) the fact that the image points within each photograph were quite well distributed, and (2) the second design matrix was a function of the radial distance. Nevertheless, it was confirmed that the image weights in the model space are

always correlated when additional parameters are used.

3.3.3 Differential Analysis

The effect of the correlation of the image weights, if not taken into account, can be evaluated both empirically and analytically. Columns (c) of tables 3.1 and 3.2 show the correlation effects on the object points and ground control points respectively. Although small in magnitude, it can be seen that the (potential) distortions occur mostly at the object points. Verifying this pattern is a typical application suitable for differential distortion analysis.

The differential distortion formula (eq. 2.28b) cannot be used here since UNBASC2 is a combined case of adjustment, as shown earlier in the chapter. Using the combined case equations in section 2.2 and following the procedure in section 2.3, the differential distortions of the solution vector due to a differential change in the weight matrix M is:

$$\frac{\partial \hat{x}}{\partial m} = -C_{\hat{X}} A^T \Delta_m (A\hat{x} + w) \qquad (3.35)$$

The analysis, confirming the pattern obtained

empirically, is performed by the following reduction. $\Delta_{\partial m}$, and thus the matrix product $C_{\hat{X}}A^T\Delta_{\partial m}$, is a tridiagonal (2x2 block for each point) matrix. Let the vector $(A\hat{x} + w)$ be partitioned into a subvector for the object points and another for the ground control points. The later is much smaller in magnitude than the former, due to their smaller values in $\hat{x}$. When multiplied by the tridiagonal matrix, the relative magnitude is preserved provided that the matrix is homogeneous. Section 7.1 shows that the ripple matrix $C_{\hat{X}}A^T$ is homogeneous. Also, from the previous section, it can be concluded that ∂m varies little between points. Therefore, $\Delta_{\partial m}$ is homogeneous. Hence, the tridiagonal matrix is homogeneous. The pattern is thus verified.

3.4 Errors and Omissions in UNBASC2

Because the original source code for UNBASC2 (version SX1) was on cards and not maintained on disk, there were a few misplaced cards that created small distortions that do not show up in the root mean square values of the image residuals, the parallaxes nor the control point residuals.

In developing the program, the first design matrix, A, was errorneous.

always correlated when additional parameters are used.

3.3.3 Differential Analysis

The effect of the correlation of the image weights, if not taken into account, can be evaluated both empirically and analytically. Columns (c) of tables 3.1 and 3.2 show the correlation effects on the object points and ground control points respectively. Although small in magnitude, it can be seen that the (potential) distortions occur mostly at the object points. Verifying this pattern is a typical application suitable for differential distortion analysis.

The differential distortion formula (eq. 2.28b) cannot be used here since UNBASC2 is a combined case of adjustment, as shown earlier in the chapter. Using the combined case equations in section 2.2 and following the procedure in section 2.3, the differential distortions of the solution vector due to a differential change in the weight matrix M is:

$$\frac{\partial \hat{x}}{\partial m} = -C_{\hat{X}} A^T \Delta_m (A\hat{x} + w) \qquad (3.35)$$

The analysis, confirming the pattern obtained

Point Number	ΔX	ΔY	ΔZ	ΔX	ΔY	ΔZ	ΔX	ΔY	ΔZ
	a) Partials			b) Double X			c) Image Weights		
1001	7	-3	1	-1	1	-2	0	1	0
1002	11	-11	8	1	0	0	0	0	0
1003	-14	3	-1	1	0	2	0	0	0
1004	15	-15	31	2	-2	5	-1	1	-2
1005	24	-26	43	4	-3	8	-2	1	-3
1006	-9	-3	1	-3	-1	0	1	0	0
1007	-1	1	8	0	0	0	0	0	1
1008	-9	0	-5	-1	0	0	1	0	0
1009	-17	-4	-21	0	0	0	0	0	0
1010	-2	-5	8	0	-1	1	0	0	0
1011	8	-31	49	1	-3	3	-1	1	0
1012	-2	-3	-3	0	1	1	0	0	0
1013	-11	-32	45	1	-1	2	0	0	-1
1014	2	4	11	0	0	1	0	0	0
1015	-1	-1	7	0	0	0	0	0	0
1016	1	4	-3	0	0	-1	1	0	0
1017	1	1	3	0	0	1	0	0	0
1018	-1	0	5	-1	0	1	0	0	-1
1019	8	7	-26	0	0	0	0	-1	1
1020	1	4	-6	-1	0	0	0	0	0
1021	0	1	1	-1	0	0	0	0	0
1022	-5	-7	-1	1	0	0	0	0	-1
1023	-1	2	-3	0	1	0	1	0	-1
1024	-4	-2	-3	0	-1	-1	1	0	-1
1025	27	13	9	0	0	1	0	0	0
1026	0	-2	-1	0	0	0	0	0	0
1027	-2	-11	20	1	0	0	0	0	-1
1028	-3	-15	29	2	0	-2	1	1	-2
1029	0	-7	0	0	1	-1	1	0	0
2147	2	0	5	1	0	1	1	0	0
2149	1	-2	3	0	0	0	0	0	0
2151	1	2	-3	0	0	0	0	0	-1
2153	2	1	-13	1	0	-2	0	0	0
2174	15	-15	20	0	-1	-1	-1	0	0
2176	-7	-3	-3	-1	0	0	0	0	1
2178	4	2	10	0	0	1	0	0	0
2180	1	3	-5	0	0	0	0	0	0
2182	2	-11	21	1	1	-1	0	1	-1
2188	0	-1	-3	0	0	0	0	0	0
2190	-18	-1	-19	0	0	1	0	0	0
2192	-6	-8	14	0	0	1	0	0	-1
2194	-4	0	-5	-1	0	0	0	0	0
2196	-9	-12	25	0	0	1	0	0	-1

Table 3.1 UNBASC2 Differential Distortions at Object Points (mm).

Point Number	ΔX	ΔY	ΔZ	ΔX	ΔY	ΔZ	ΔX	ΔY	ΔZ
	a) Partials			b) Double X			c) Image Weights		
5111	0	0	0	0	0	0	0	0	0
5112	0	0	0	1	0	0	0	0	0
5114	0	0	0	0	0	0	0	0	0
5115	0	0	0	0	0	0	0	0	0
5117	0	0	0	-1	0	0	0	0	0
5120	0	0	0	0	0	0	0	0	0
5122	0	0	0	0	0	0	0	0	0
5123	0	0	0	0	0	0	0	0	0
5124	0	0	0	1	0	0	0	0	0
5125	0	-1	0	0	0	0	0	0	0
5127	0	0	0	0	0	0	0	0	0
5130	0	0	0	0	0	0	0	0	0
5131	0	0	0	0	0	0	0	0	0
5156	0	0	0	0	0	0	0	0	0
5157	0	0	0	0	0	0	0	0	0
5158	0	0	0	-1	0	0	0	0	0
5220	0	0	0	0	0	0	0	0	0
5221	0	0	0	1	0	0	0	0	0
5222	0	0	0	0	0	0	0	0	0
5223	0	0	0	-1	0	0	0	0	0
5224	0	0	0	0	0	0	0	0	0
5314	0	0	0	0	0	0	0	0	0
5315	0	0	0	0	0	0	0	0	0
5417	0	0	0	1	0	0	0	0	0
7018	-6	-2	0	-1	-1	0	0	0	0
7019	0	-2	0	0	0	0	0	1	0
7116	-14	-4	0	0	0	0	0	0	0
7119	-5	1	0	0	0	0	0	0	0

Table 3.2 UNBASC2 Differential Distortions at Control Points. Horizontal control points (5111 to 5417) and vertical control points (7018 to 7119) were used. Edmunston test data: scale = 1/7800, c = 151.35 and targeted full control (standard deviation 5 to 10 cm) were used. Expected standard deviation of adjusted coordinates = 5 micrometres (image) = 4 cm (object).

3.4.1 Y Residuals

One of the errors in UNBASC2 was that of potentially erroneous residuals. A misplaced card (subroutine OUTPUT ISN 271 & 273) resulted in the contribution to the y residuals being skipped. However, this does not happen if the image weights M are correlated.

As shown in section 3.3, the weights are always correlated if additional parameters are used. Therefore, the y residuals were computed properly. The effect on adjustments without additional parameters was not studied.

3.4.2 Double X Normals

Another error in the program, due to duplicated cards (subroutine ADJUST ISN 176 & 177), resulted in the doubling of the ground control point x-contributions to the normal equations. This is equivalent to doubling the weight of the x coordinates of the ground control points.

The effect of the double weights on the adjusted coordinates (columns (b) of tables 3.1 and 3.2) was again quite small. Differential distortion analysis may be used to verify the results. Eq. (2.29b) is valid for both the

combined and the parametric cases.

With the expected precision from the bundle adjustment (4 cm) in the same order of magnitude as the estimated precision of the ground control points, their covariance matrix is probably highly correlated (see chapters 5 and 6). If that is so, it could be the reason why ΔY and ΔZ at the control points are zero.

3.5 Defect in the Design Matrices

Eq. (3.5) clearly shows that the additional parameters are functions of the radial distance of the image points. However, in taking the partial derivatives (equations 3.14 & 3.16) Moniwa (1977) did not include the partial derivatives of the radial distance. The design matrices were rederived to overcome this defect. The defect is analyzed using the Edmunston test block.

3.5.1 UNBASC2 Modified Partial Derivitives

From eq. (3.6), the partial derivatives of r are:

$$\frac{\partial r}{\partial x} = 0.5((x - x_o)^2 + (y - y_o)^2)^{-0.5}\, 2(x - x_o)$$

$$= \frac{(x - x_o)}{r} \qquad (3.36a)$$

$$\frac{\partial r}{\partial y} = \frac{(y - y_o)}{r} \tag{3.36b}$$

$$\frac{\partial r}{\partial x_o} = - \frac{(x - x_o)}{r} \tag{3.36c}$$

$$\frac{\partial r}{\partial y_o} = - \frac{(y - y_o)}{r} \tag{3.36d}$$

Therefore, the modified partial derivatives of the photogrametric functional model with respect to the image unknown and the principal point should be as follows (additional terms due to modifications are underscored):

$$\frac{\partial F_{p_x}}{\partial x} = 1 + (k_1 r^2 + k_2 r^4 + k_3 r^6) + 4p_1(x - x_o) + 2p_2(y - y_o)$$

$$\underline{+ 2(x - x_o)^2(k_1 + 2k_2 r^2 + 3k_3 r^4) + 2p_1(x - x_o)} \tag{3.37a}$$

$$= - \frac{\partial F_{p_x}}{\partial x_o} \tag{3.38a}$$

$$\frac{\partial F_{p_x}}{\partial y} = 2p_2(x - x_o) + A$$

$$\underline{+ 2(x - x_o)(y - y)(k_1 + 2k_2 r^2 + 3k_3 r^4) + 2p_1(y - y_o)} \tag{3.37b}$$

$$= - \frac{\partial F_{p_x}}{\partial y_o} \tag{3.38b}$$

$$\frac{\partial F_{p_y}}{\partial x} = 2p_1(y-y_o)$$

$$+ 2(x-x_o)(y-y_o)(k_1+2k_2r^2+3k_3r^4) + 2p_2(x-x_o) \qquad (3.37c)$$

$$= - \frac{\partial F_{p_y}}{\partial x_o} \qquad (3.38c)$$

$$\frac{\partial F_{p_y}}{\partial y} = 1 + (k_1r^2+k_2r^4+k_3r^6) + 4p_2(y-y_o) + 2p_1(x-x_o)$$

$$+ 2(y-y_o)^2(k_1+2k_2r^2+3k_3r^4) + 2p_2(y-y_o) \qquad (3.37d)$$

$$= - \frac{\partial F_{p_y}}{\partial y_o} \qquad (3.38d)$$

3.5.2 Effects of Defect in Design Matrices

The modified partial derivatives were compared with the original ones. Fig. 3.1 illustrates their differences at various radial distances from the principal point and at a polar angle of forty five degrees. Effects of the defect on the solution vector can be expressed analytically and empirically. Differential distortion analysis gives

$$\frac{\partial \hat{x}}{\partial a} = - C_{\hat{X}}A^TM\Delta_a^T\hat{x} - C_{\hat{X}}\Delta_aM(A\hat{x} + w) \qquad (3.39)$$

$$\frac{\partial \hat{x}}{\partial b} = C_{\hat{X}}A^TM^{-1}(\Delta_bC_rB^T + BC_r\Delta_b^T)M^{-1}(A\hat{x} + w) \qquad (3.40)$$

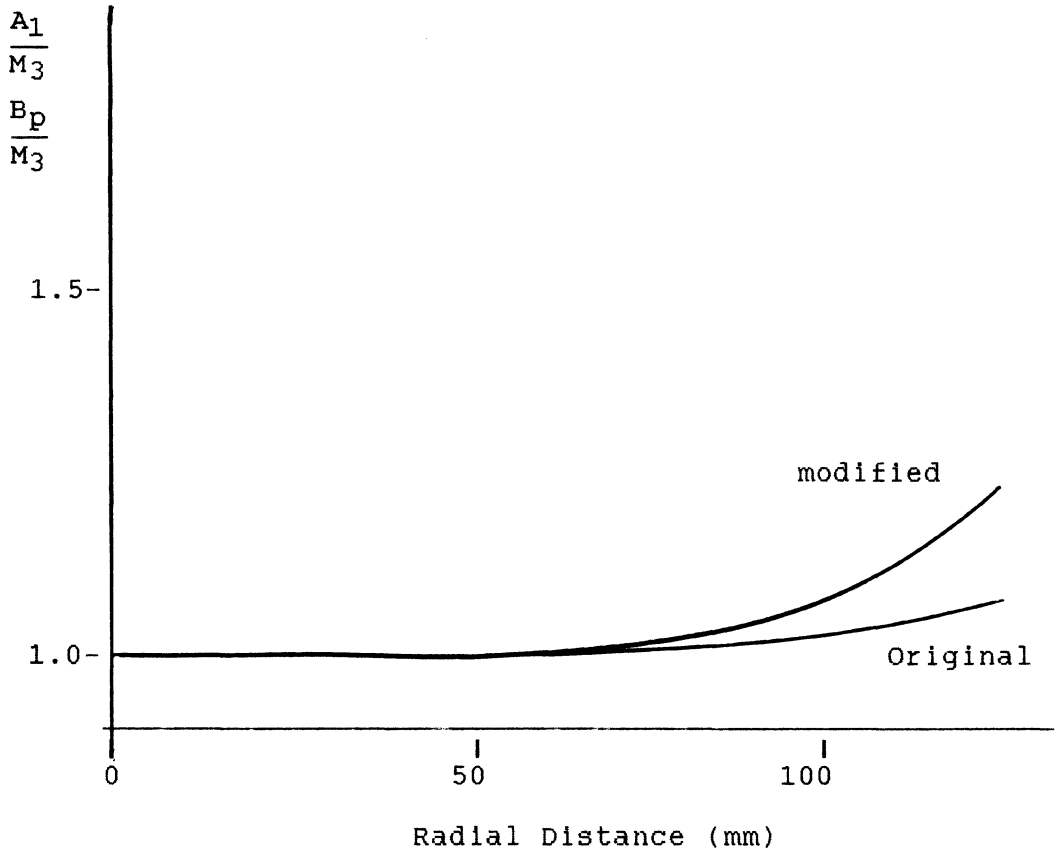

Fig. 3.1 UNBASC2 Design Matrix Function:
$k_1 = 10^{-6}$ $k_2 = 10^{-10}$ $k_3 = 10^{-14}$
$p_1 = 10^{-5}$ $p_2 = 10^{-5}$ A = 0.0025 B = 0.0015
At the polar angle of 45 degrees,

$$\frac{\partial F_x}{\partial x} = \frac{\partial F_y}{\partial y} = -\frac{\partial F_x}{\partial x_o} = -\frac{\partial F_y}{\partial y_o}$$

Differential distortions due to the defect in the design matrices were empirically obtained by repeating the adjustment with the modified partial derivatives. Results obtained are shown in columns (a) of tables 3.1 and 3.2. The maximum distortions are 27, 32 and 49 mm in X, Y and Z respectively. At the image, these correspond to 3.4, 4.1 and 6.2 micrometres. The root mean square values of the distortions are 7, 8 and 13 mm (object) or 0.9, 1.0 and 1.7 micrometres (image) in X, Y and Z respectively.

These significant distortions are systemmatic, as shown in Fig. 3.2, where pairs of horizontal distortion vectors of similar magnitude and direction are evident. Note in particular the pairs at points (1002, 2174); (2190, 1009); (2196, 1027) and (1008, 2176). Similarly, pairs of vertical distortion vectors are also evident.

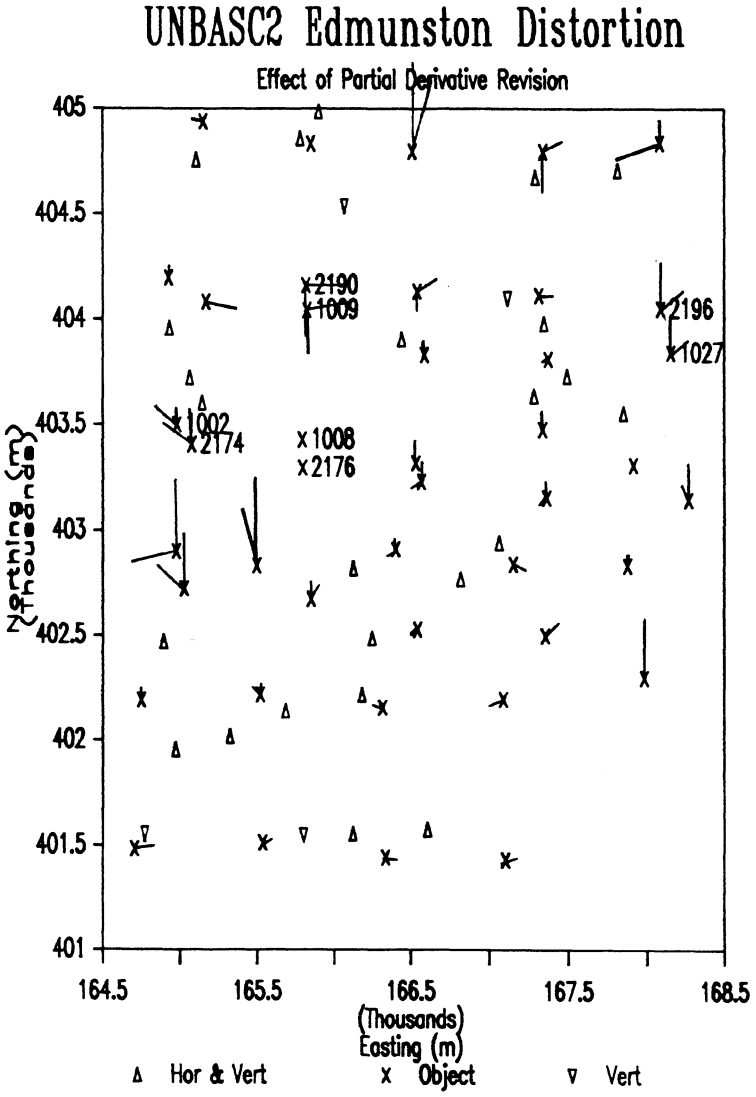

Scale of distortion vectors: 0 +------+ 10 cm

Fig. 3.2 UNBASC2 Edmonston Distortion. Systematic effect of neglecting the partial derivatives of the radial distance with respect to the image coordinates and the principal point.

CHAPTER IV

GEBAT DIFFERENTIAL DISTORTION

GEBAT (El-Hakim, 1979) is another bundle adjustment program with self calibration. Although the same functional model - the collinearity equations - is used as in UNBASC2, the additional parameters are different. The generalized additional parameters are coefficients of a harmonic function.

There are different versions of GEBAT, all of which contain an additional geodetic functional model. This allows distances between object points as observations. The version GEBATV, which is photo-variant, was examined. This version also features data-snooping and error ellipsoid output.

A defect similar to UNBASC2 was found in GEBATV. The

partial derivatives in the second design matrix took into account that the radial distance is a function of the position of the image points. However, this consideration was omitted in the partial derivatives of the first design matrix. The differential distortion caused by this defect is examined below.

4.1 GEBAT Photogrammetric Functional Model

The collinearity equations modified for additional parameters are expressed in GEBAT as follows:

$$F_x = (x - x_o) + (x - x_o)T + c\,\frac{M_1}{M_3} = 0 \qquad (4.1a)$$

$$F_y = (y - y_o) + (y - y_o)T + c\,\frac{M_2}{M_3} = 0 \qquad (4.1b)$$

with the distortion being modelled by the harmonic function

$$\begin{aligned} T = {} & a_{00} + a_{11}\cos\lambda + b_{11}\sin\lambda + a_{20}r + a_{22}r\cos 2\lambda \\ & + b_{22}r\sin 2\lambda + a_{31}r^2\cos\lambda + b_{31}r^2\sin\lambda \\ & + a_{33}r^2\cos 3\lambda + b_{33}r^2\sin 3\lambda \end{aligned} \qquad (4.2)$$

where a and b are the harmonic coefficients, r is the radial distance as in eq. (3.6) and λ is given by:

$$\lambda = \tan^{-1}\frac{(y - y_o)}{(x - x_o)} \qquad (4.3)$$

4.2 GEBAT Design Matrix Defect

Taking into account that the radial distance is a function of (x, y) and (x_o, y_o), the following partial derivatives in the first design matrix of GEBAT are revised

$$\frac{\partial F_{p_x}}{\partial x_o} = - M_3 - TM_3 \underline{- (x-x_o)T_5M_3} \tag{4.4}$$

$$\frac{\partial F_{p_x}}{\partial y_o} = \underline{- (x-x_o)T_6M_3} \tag{4.5}$$

$$\frac{\partial F_{p_y}}{\partial x_o} = \underline{- (y-y_o)T_5M_3} \tag{4.6}$$

$$\frac{\partial F_{p_y}}{\partial y_o} = - M_3 - TM_3 \underline{- (y-y_o)T_6M_3} \tag{4.7}$$

where

$$\begin{aligned} T_5 = \frac{\partial T}{\partial x_o} = -(&a_{11}\frac{\sin^2\lambda}{r} - b_{11}\frac{\cos\lambda\sin\lambda}{r} + a_{20}\cos\lambda \\ &+ a_{22}(2\sin 2\lambda\sin\lambda + \cos 2\lambda\cos\lambda) \\ &+ b_{22}(\sin 2\lambda\cos\lambda - 2\sin\lambda\cos 2\lambda) \\ &+ a_{31}(r + (x-x_o)\cos\lambda) + b_{31}(x-x_o)\sin\lambda) \end{aligned} \tag{4.8}$$

$$\begin{aligned} T_6 = \frac{\partial T}{\partial y_o} = -(&-a_{11}\frac{\cos\lambda\sin\lambda}{r} + b_{11}\frac{\cos^2\lambda}{r} + a_{20}\sin\lambda \\ &+ a_{22}(\cos 2\lambda\sin\lambda - 2\sin 2\lambda\cos\lambda) \\ &+ b_{22}(\sin 2\lambda\sin\lambda - 2\cos\lambda\cos 2\lambda) \\ &+ a_{31}(x-x_o)\sin\lambda + b_{31}(r + (y-y_o)\sin\lambda)) \end{aligned} \tag{4.9}$$

In the above partial derivatives of equations (4.4 to 4.7), the underlined portions were missing from the program. With the revision, the expected relationships:

$$\frac{\partial F_p}{\partial x_o} = - \frac{\partial F_p}{\partial x} \quad \text{and} \quad \frac{\partial F_p}{\partial y_o} = - \frac{\partial F_p}{\partial y} \tag{4.10}$$

are obtained as they should clearly have been. This is easily seen by inspection of eq. (4.1).

4.3 Effect of Defect in Design Matrix

The effect of these missing terms in the design matrix was negligible in the test data set supplied with the program. Using the adjusted harmonic coefficients, the contribution to the design matrix (scaled by M3) is shown in Fig. 4.1. While the amount of distortion varies with λ and r, it can be seen that 50% to 100% of the intended modelling was missed. However, closer examination of equations (4.4 to 4.9) shows that the missing terms are merely second order, being derivatives of the harmonic function (eq. 4.3). Hence, the negligible effect on the test data set.

Analytically, the defect caused a differential distortion as given by eq. (3.39).

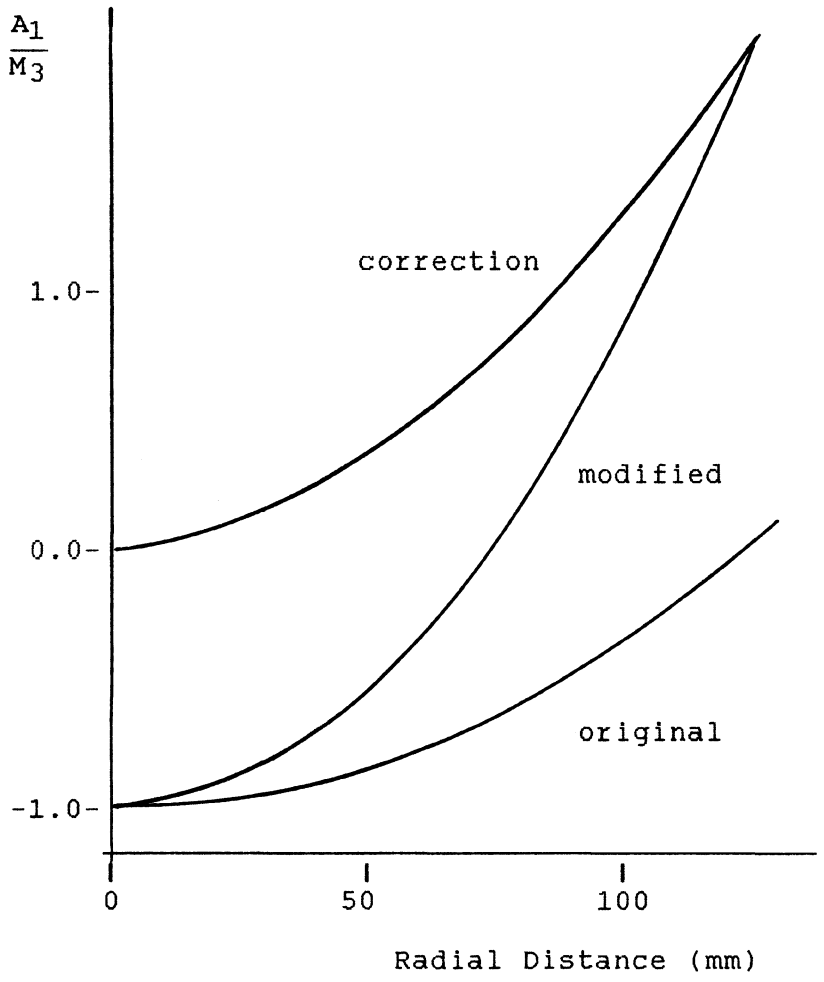

Fig. 4.1 GEBAT Design Matrix Function:

a_{00} = 0.001844 a_{11} = -0.000387
b_{11} = -0.000241 a_{20} = -0.000247
a_{22} = 0.001167 b_{22} = 0.000426
a_{31} = -0.000100 b_{31} = -0.000078

At the polar angle of 45 degrees,

$$\frac{\partial F_x}{\partial x} = \frac{\partial F_y}{\partial y} = -\frac{\partial F_x}{\partial x_o} = -\frac{\partial F_y}{\partial y_o}$$

CHAPTER V

CASE STUDIES OF HIGHLY CORRELATED COVARIANCE MATRICES

In several instances where the covariance matrices of the adjusted parameters were available, their correlation matrices were examined. In all cases, high correlation in the covariance matrices were evident when the densification observations were of the same precision or better than the control network coordinates. The following are cases of production projects where these occur:

5.1 LEAP ATS77 Readjustment

271 federal control points were weighted in the LEAP simultaneous parametric adjustment of 40887 LRIS stations (Nickerson, 1981). The mean value of the major semiaxes of the standard error ellipses for the 271 weighted stations is 24.6 cm

before and 2.7 cm after the readjustment. The averages for the New Brunswick portion of the network (18017 stations) are 6.0 $\pm$ 4.0 cm (Voon, 1982).

From samples of the already computed covariance submatrices (see Figs 5.1 to 5.3) it can be seen that all the latitudes are highly correlated at 98%. Similarly, all longitudes are just as highly correlated. However, longitudes and latitudes are not significantly correlated. Mean station correlation is zero (Table 5.1), with 95% of the station ϕ/λ autocorrelation being insignificant.

There is no tendency for precision to deteriorate towards the edge of the network. Taking the ratio of the standard deviation of position of each station over its distance to the center of the network, the precision of the New Brunswick stations is tabulated. Table 5.1 shows that the precision is not constant. Thus, the positional error is not a linear function of the distance from the geographic center of the network.

From the above data and interpretations, it is hypothesized that the correlation pattern prevails throughout the whole covariance matrix.

ø	λ	ø	λ	ø	λ	ø	λ	ø	λ
1.90	-.34	1.90	-.26	1.70	-.22	1.76	-.21	1.87	-.36
	2.38	-.35	2.26	-.24	2.27	-.26	2.27	-.30	2.39
		1.97	-.23	1.67	-.18	1.73	-.19	1.84	-.38
			2.48	-.35	2.32	-.34	2.34	-.34	2.20
				1.94	-.47	1.90	-.46	1.75	-.21
					2.63	-.43	2.59	-.25	2.25
						1.90	-.42	1.79	-.24
							2.61	-.24	2.25
								1.95	-.29
symmetric									2.55

ø	λ	ø	λ	ø	λ	ø	λ	ø	λ
1	-.02	.98	-.12	.89	-.12	.92	-.09	.97	-.16
	1	-.16	.93	-.11	.91	-.12	.91	-.14	.97
		1	-.10	.86	-.08	.90	-.08	.94	-.17
			1	-.16	.91	-.16	.92	-.16	.88
				1	-.21	.99	-.21	.90	-.12
					1	-.19	.99	-.11	.87
						1	-.19	.93	-.11
							1	-.11	.87
								1	-.13
symmetric									1

Fig. 5.1 ATS77 Subnet 14 Correlation. Covariance (ms^2) and correlation submatrix for LRIS stations 110590, 110591, 110685, 110686 and 110744

ϕ	λ	ϕ	λ	ϕ	λ	ϕ	λ
2.22	-.12	2.11	-.09	2.00	-.08	1.951	-.08
	4.74	-.10	4.61	-.12	4.21	-.12	4.07
		2.13	-.12	2.01	-.10	1.96	-.08
			4.59	-.12	4.23	-.12	4.10
				2.14	-.15	2.04	-.10
					4.29	-.11	4.20
						2.06	-.11
symmetric							4.23

ϕ	λ	ϕ	λ	ϕ	λ	ϕ	λ
1	-.04	.97	-.03	.92	-.03	.91	-.03
	1	-.03	.99	-.04	.93	-.04	.91
		1	-.04	.94	-.03	.94	-.03
			1	-.04	.95	-.04	.93
				1	-.05	.97	-.04
					1	-.02	.99
						1	-.04
symmetric							1

Fig. 5.2 ATS77 Subnet 06 Correlation. Covariance (ms^2) and correlation submatrix for LRIS Stations 301595, 301594, 301592 and 301562.

ø	λ	ø	λ	ø	λ
2.38	-.49	2.15	-.42	1.99	-.37
	4.11	-.36	3.77	-.29	3.48
		2.05	-.29	1.95	-.29
			3.75	-.26	3.47
				1.90	-.23
symmetric					3.48

ø	λ	ø	λ	ø	λ
1	-.16	.97	-.14	.93	-.13
	1	-.13	.96	-.10	.93
		1	-.11	.98	-.11
			1	-.10	.96
				1	-.09
symmetric					1

Fig. 5.3 ATS77 Subnet 05 Correlation. Covariance (ms^2) and correlation submatrix for LRIS Stations 113926, 113927 and 113928

Class No.	Station ϕ/λ Correlation Range	Count	Sigma Position (cm) Range	Count	Precision (ppm) Range	Count
1	(-1.0,-0.9)	3	(0, 2)	0	(0.0,0.2)	327
2	(-0.9,-0.8)	93	(2, 4)	251	(0.2,0.4)	5984
3	(-0.8,-0.7)	78	(4, 6)	6164	(0.4,0.6)	7342
4	(-0.7,-0.6)	72	(6, 8)	6956	(0.6,0.8)	2355
5	(-0.6,-0.5)	166	(8,10)	2275	(0.8,1.0)	804
6	(-0.5,-0.4)	293	(10,12)	921	(1.0,1.2)	555
7	(-0.4,-0.3)	525	(12,14)	459	(1.2,1.4)	291
8	(-0.3,-0.2)	1216	(14,16)	332	(1.4,1.6)	125
9	(-0.2,-0.1)	3992	(16,18)	260	(1.6,1.8)	73
10	(-0.1, 0.0)	3912	(18,20)	113	(1.8,2.0)	86
11	(0.0, 0.1)	4401	(20,22)	70	(2.0,2.2)	41
12	(0.1, 0.2)	1683	(22,24)	53	(2.2,2.4)	18
13	(0.2, 0.3)	729	(24,26)	38	(2.4,2.6)	1
14	(0.3, 0.4)	310	(26,28)	20	(2.6,2.8)	5
15	(0.4, 0.5)	230	(28,30)	26	(2.8,3.0)	1
16	(0.5, 0.6)	196	(30,32)	23	(3.0,3.2)	0
17	(0.6, 0.7)	102	(32,34)	9	(3.2,3.4)	2
18	(0.7, 0.8)	13	(34,36)	7	(3.4,3.6)	1
19	(0.8, 0.9)	0	(36,38)	5	(3.6,3.8)	3
20	(0.9, 1.0)	3	(38...)	35	(3.8 ...)	3
Mean	-0.0		7.5		0.5	
Sigma	0.2		4.3		0.3	
Minimum	-1.0		2.5		0.1	
Maximum	1.0		177.8		7.0	

Table 5.1 New Brunswick Network Precision. Histograms of 1) station correlation coefficients, 2) standard deviation of position and 3) precision relative to the center of the ATS77 network of 18017 New Brunswick stations. These are obtained from the ATS77 unscaled (a-posteriori variance factor = 2.3) variance-covariance matrix of the adjusted coordinates.

5.2 GEODOP Doppler Correlation

The correlation matrix of the adjusted coordinates (Shell, 1978) from program GEODOP is shown in Fig. 5.4. Notice the pattern of high latitude-latitude and longitude-longitude correlation similar to that of the ATS77.

5.3 GLDSAT Macrometer Densification

Seven new stations were adjusted to four control stations weighted at 1 m. The 3D adjustment program GLDSAT was modified (Hosford et al, 1983) to accept position differences of Macrometer observations with a standard deviation of 3 cm. The adjusted coordinates had standard deviations of 46 cm in latitude and in longitude. The covariance matrix again shows very high (99%) station cross-correlation (see Fig. 5.5) similar to the pattern in the ATS77 covariance matrix.

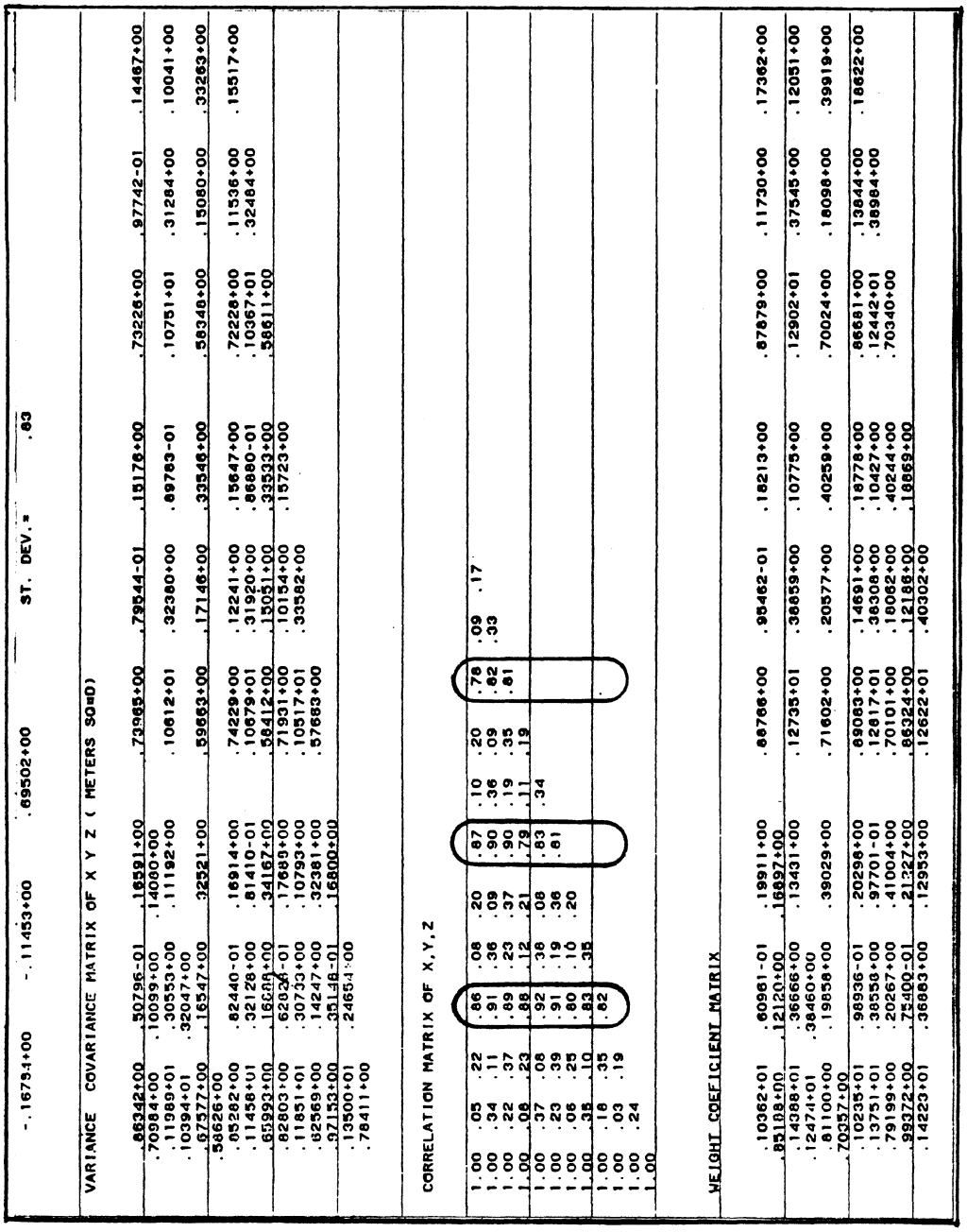

-.16754+00 -.11453+00 .69502+00 ST. DEV.* .83

VARIANCE COVARIANCE MATRIX OF X Y Z (METERS SQ=D)

.86342+00	.50795-01	.16591+00	.73985+00	.79544-01	.18176+00	.73226+00	.97742-01	.14467+00			
.70984+00	.10099+00	.14080+00									
.11989+01	.30553+00	.11192+00	.10612+01	.32380+00	.89783-01	.10751+01	.31284+00	.10041+00			
.10394+01	.32047+00										
.67577+00	.16547+00	.32521+00	.59553+00	.17148+00	.33548+00	.58348+00	.15080+00	.33263+00			
.58626+00											
.05282+00	.82440-01	.16914+00	.74229+00	.12241+00	.15647+00	.72228+00	.11536+00	.15517+00			
.11458+01	.32128+00	.81410-01	.10679+01	.31920+00	.86880-01	.10367+01	.32484+00				
.65993+00	.16088+00	.34167+00	.58412+00	.15051+00	.33533+00	.56611+00					
.82803+00	.62836-01	.17689+00	.71931+00	.10154+00	.15723+00						
.11851+01	.30733+00	.10793+00	.10517+01	.33582+00							
.82569+00	.14247+00	.32381+00	.57683+00								
.97153+00	.35148-01	.16800+00									
.13500+01	.24654+00										
.78411+00											

CORRELATION MATRIX OF X,Y,Z

1.00	.05	.22	.86	.08	.20	.87	.10	.20	.78	.09	.17
1.00	.34	.11	.91	.36	.09	.90	.36	.09	.82	.33	
1.00	.22	.37	.89	.23	.37	.90	.19	.35	.81		
1.00	.08	.23	.88	.12	.21	.79	.11	.19			
1.00	.37	.08	.92	.36	.08	.83	.34				
1.00	.23	.39	.91	.19	.36	.81					
1.00	.06	.25	.80	.10	.20						
1.00	.35	.10	.83	.35							
1.00	.18	.35	.82								
1.00	.03	.19									
1.00	.24										
1.00											

WEIGHT COEFICIENT MATRIX

.10362+01	.60961-01	.19911+00	.88766+00	.95462-01	.18213+00	.87879+00	.11730+00	.17362+00
.83108+00	.12120+00	.16897+00						
.14388+01	.36666+00	.13431+00	.12735+01	.38659+00	.10775+00	.12902+01	.37545+00	.12051+00
.12474+01	.38460+00							
.81100+00	.19858+00	.39029+00	.71602+00	.20577+00	.40259+00	.70024+00	.18098+00	.39919+00
.70357+00								
.10235+01	.98936-01	.20298+00	.89083+00	.14691+00	.18778+00	.86681+00	.13844+00	.18622+00
.13751+01	.38558+00	.97701-01	.12817+01	.38308+00	.10427+00	.12442+01	.38984+00	
.79199+00	.20267+00	.41004+00	.70101+00	.18062+00	.40244+00	.70340+00		
.99372+00	.75400-01	.21327+00	.89324+00	.12198+00	.18869+00			
.14223+01	.36883+00	.12953+00	.12622+01	.40302+00				

Fig. 5.4 GEODOP Correlation. All X's are highly correlated. Similarly, all Y's are highly correlated and all Z's are highly correlated. However, correlation between parameters are insignificant.

∅	λ	H	∅	λ	H	∅	λ	H
1	-0	.04	.99	-0	0	.99	-0	.04
	1	.03	0	.99	-0	0	.99	-.04
		1	.04	.03	.36	.04	.03	.47
			1	0	0	.99	-0	.05
				1	-0	0	.99	-.05
					1	0	-0	.36
						1	0	.05
							1	-.04
symmetrical								1

Fig. 5.5 GLDSAT Correlation. Correlation submatrix for Crownest Macrometer stations Center, CR-03 and Allison. ∅'s are highly correlated among themselves. So are λ's. However, H's are only moderately correlated. Between ∅, λ and H, the correlation is insignificant. The same correlation pattern persists throughout the entire covariance matrix of all 11 stations. The horizontal component of this correlation matrix is similar to the pattern in the LRIS ATS77 covariance matrix.

CHAPTER VI

PHOTOGRAMMETRIC HIGH CORRELATION SIMULATION

In order to demonstrate that a similarly high correlation can result from a photogrammetric bundle adjustment, a preanalysis was conducted with the program BMAC which produces the covariance matrix of the adjusted parameters. As the full covariance matrix was computed, it was necessary to limit the size of the test data.

A two photo simulation was used with 25 points, 5 of which were control points. Standard deviations of the ground control points were varied from 0.0001 m to 100 m while the standard deviation of the image coordinate observations was maintained at 6 micrometres.

High correlation of the pattern discussed in chapter

V was found to occur. That is, the X (or Y or Z) correlation between the object points could be very high. Similarly, the correlation of exterior orientation elements between the photographs could also be very high. Correlations between the different parameters were mostly lower.

6.1 Correlation Between Object Points

Shown in Fig. 6.1 is a plot for the correlation of the Z coordinates of all the points with respect to point 24. As is evident, there is high correlation when the control coordinates were much less precise than the photogrammetric observations, which have expected precision of 0.01 m.

It is interesting to note that the curve for 10 m shows about the same shape as that of the 0.01 m curve. It may be that at a certain point, the influence of the control is sufficiently relaxed to allow the densification to maintain a best fit. This control relaxation point seems to be reached when the ratio of the precisions of image and ground control points is between 100 and 1000. Compared to the ATS77 ratio of 10 (section 5.1), this seems to be quite high

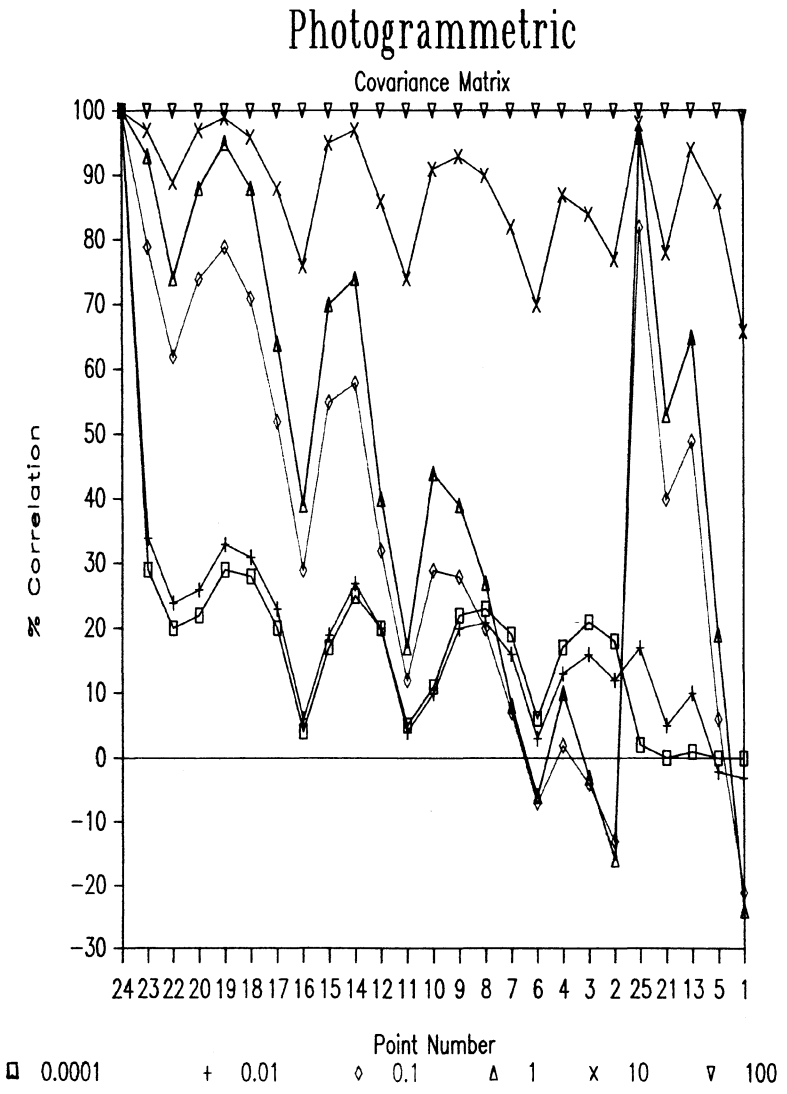

Fig 6.1 Photogrammetric Correlation Preanalysis. Z correlation, reference point 24, with increasing standard deviation of ground control points increasing from 0.0001 to 100 m. Expected photogrammetric precision = 0.01 m. 1, 5, 13, 21, 25 are the ground control points.

6.2 Correlation Between Exterior Orientation Elements

Exterior orientation parameters became mutually correlated between photo 1 and 2 as the standard deviations of the ground control points were increased. The results are summarized in Table 6.1.

Photo 1,2	$\sigma X_g = \sigma Y_g = \sigma Z_g$ (m)						
	0.0001	0.001	0.01	0.1	1	10	100
X_C	8	9	48	88	98	91	99
Y_C	7	9	47	86	94	82	61
Z_C	11	11	17	88	92	98	100
κ	47	48	81	100	100	100	100
ϕ	7	8	48	89	100	100	100
ω	7	8	47	91	100	100	100

Table 6.1 Exterior Orientation Parameter Correlation. Percentage correlation of exterior orientation parameters of photos 1 and 2 with increasing standard deviation of ground control points

CHAPTER VII

IMPLICATIONS OF HIGHLY CORRELATED CONTROL

In light of the cause and effect of the highly correlated covariance matrix, some issues in densification by photogrammetric bundle adjustment are raised below:

(1) As the precision of photogrammetric densification approaches that of the geodetic networks to be densified, the densification covariance matrix is expected to be highly correlated, giving rise to global ripple effects.

(2) With highly correlated ground control points, their relative precision should be considered in weighting bundle adjustments.

(3) Alternative covariance matrices to reduce costs are investigated. The selected alternative covariance matrices for the ground control points should provide acceptable distortions in the adjusted coordinates.

(4) The choice of an apriori covariance matrix should provide a suitable aposteriori covariance matrix of the densification to allow proper statistical assessment of the changes in the coordinates of the weighted stations.

7.1 Ripple Effects of A Highly Correlated Covariance Matrix

Positional errors from the ATS77 readjustment are of the same order of magnitude as the precision obtainable by photogrammetric densification. The mean of the vector sum of standard deviations of ϕ and λ in the New Brunswick portion of the network is 7.5 $\pm$ 4.3 cm (see table 5.1). In contrast, El-Hakim (1982) reported a precision obtainable by photogrammetric densification with bundle adjustment of two centimetres, at a photo scale of 1:4400. Therefore, a bundle adjustment densification of the New Brunswick network would likely produce a highly correlated covariance matrix.

In production, it is quite common to discover blunders after a project has been approved and the coordinates published. The effect of the blunders may be studied with the differential distortion analysis developed in chapter 2. The analysis hinges on the nature of the covariance matrix of the adjusted parameters.

$\frac{\partial \hat{x}}{\partial t}$ of eq. (2.21) may be termed the ripple effect. This is the degree of change in the adjusted coordinates due to changes in the adjustment variables. In fixed adjustments, the covariance matrix of the adjusted parameters is usually diagonally dominant. Therefore, the ripple effects of local distortions rapidly decrease with increasing distance from the cause of the distortions. However, when the covariance matrix is of the highly correlated pattern (as shown in section 5.1), the ripple effects are no longer localized. The distortions are spread throughout the solution vector. This can be seen from the matrix product $N^{-1}A^T$ which has a structure of:

$$
\begin{bmatrix}
* & 0 & * & 0 & * & 0 & * & 0 & * & 0 & * & 0 \\
 & * & 0 & * & 0 & * & 0 & * & 0 & * & 0 & * \\
 & & * & 0 & * & 0 & * & 0 & * & 0 & * & 0 \\
 & & & * & 0 & * & 0 & * & 0 & * & 0 & * \\
 & & & & * & 0 & * & 0 & * & 0 & * & 0 \\
 & & & & & * & 0 & * & 0 & * & 0 & * \\
 & & & & & & * & 0 & * & 0 & * & 0 \\
 & & & & & & & * & 0 & * & 0 & * \\
 & & & & & & & & * & 0 & * & 0 \\
 & & & & & & & & & * & 0 & * \\
 & & & & & & & & & & * & 0 \\
\text{symmetric} & & & & & & & & & & & *
\end{bmatrix}
\begin{bmatrix}
0 & 0 & 0 & \ldots & x \\
0 & 0 & 0 & \ldots & x \\
0 & -x & x & \ldots & 0 \\
0 & -x & x & \ldots & 0 \\
0 & 0 & 0 & \ldots & -x \\
0 & 0 & 0 & \ldots & -x \\
-x & 0 & -x & \ldots & 0 \\
-x & 0 & -x & \ldots & 0 \\
0 & x & 0 & \ldots & 0 \\
0 & x & 0 & \ldots & 0 \\
x & 0 & 0 & \ldots & 0 \\
x & 0 & 0 & \ldots & 0
\end{bmatrix}
$$

N is of dimension u by u while A is n by u. The product is a u by n 'ripple matrix' that is fully populated, even though A may be very sparse. Moreover, the ripple matrix has elements that are very small in magnitude due to cancellations in the summation during matrix multiplication. The cancellation occurs because of the alternating positive and negative terms in the columns of A^T. The elements of the ripple matrix are homogeneous if the elements of A are of the same order of magnitude.

The global ripple effects can be observed in the results of the test network of section 7.3.3. Distortions in the entire solution vector, due to changes in the apriori covariance matrix, is clearly seen in Table 7.1.

7.2 Relative Precision of Ground Control Points

With a highly correlated covariance matrix, relative error ellipses indicate the precision of the network much better than absolute error ellipses. The mean value of the major semiaxes of the standard relative error ellipses for the 22321 sightlines in New Brunswick is 1.6 $\pm$ 3.3 cm while that of the absolute error ellipses is 6.0 $\pm$ 4.0 cm (Voon, 1984). In comparison, the mean standard deviation of the adjusted distances is 1.4 $\pm$ 3.2 cm, agreeing better with the relative ellipses.

Since the geodetic control points can be so highly correlated, densification adjustments using intra-station (auto) covariances but not inter-station (cross) covariances do not account for the more significant information on their relative precision. This is a common mistake in weighting (Hamilton, 1964) which can lead to differential distortions in the adjusted coordinates as given by eq. (2.29b). The estimates of the variances can be more severely effected (equations 2.29a, c,& e).

Few programs allow the inter-station covariances in order to optimize their data structure. The structure of the photogrammetric block adjustment normal equations is

very sparse. Special techniques, such as Cholesky block factorization, are often used to take advantage of this. In programs that are highly optimized, the inclusion of weights (even 3x3 station covariance matrices) for the ground control points do not pose a problem. However, if the ground control inter-station covariance information is to be introduced into the block adjustment, the numerical processing has to take on a different strategy and may not be as straightforward to implement (Moniwa, 1980).

To solve the numerical problem, Brown (1974) proposed the banded-bordered form of recursive partitioning. For programs that cannot accept the full covariance matrix of the ground control points, two solutions could be investigated. One is the use of relative coordinates of the ground control points (Blais & Chapman, 1983) along with covariance transformation (Hees, 1982 and Molenaar, 1981). The other is decorrelation of the ground control points (Milbert, 1985).

7.3 Alternative Apriori Covariance Matrices

The covariance matrix of the adjusted parameters can be very expensive to generate for a regional geodetic

network. The cost, alternatives and results of using artificial covariance matrices were studied.

7.3.1 Cost of ATS77 Covariance Data

The ATS77 readjustment produced the covariance matrix within the profile (Nickerson, 1981) at a reasonable cost. Extracting elements of the covariance matrix that are with the profile cost between $2 to $5. However, obtaining off-profile elements can still be relatively expensive. Fig. 7.1 shows the location in the covariance matrix from which off-profile elements of the submatrix (Fig. 5.1) were computed. Even though the position of the stations were within 20 of each other in the normal equations, the computation cost was $373 (Nickerson & Knight, 1983). In comparison, a block of 1000 points can be adjusted (including all production reruns) with PATM-43 for $700 on the same computer installation. Other submatrices may be computed quite inexpensively. The costs of computing the submatrices shown in Figures 5.2 and 5.3 were respectively $22 and $17.

7.3.2 Artificial Covariance Matrices

Due to the high cost of computing the off-profile

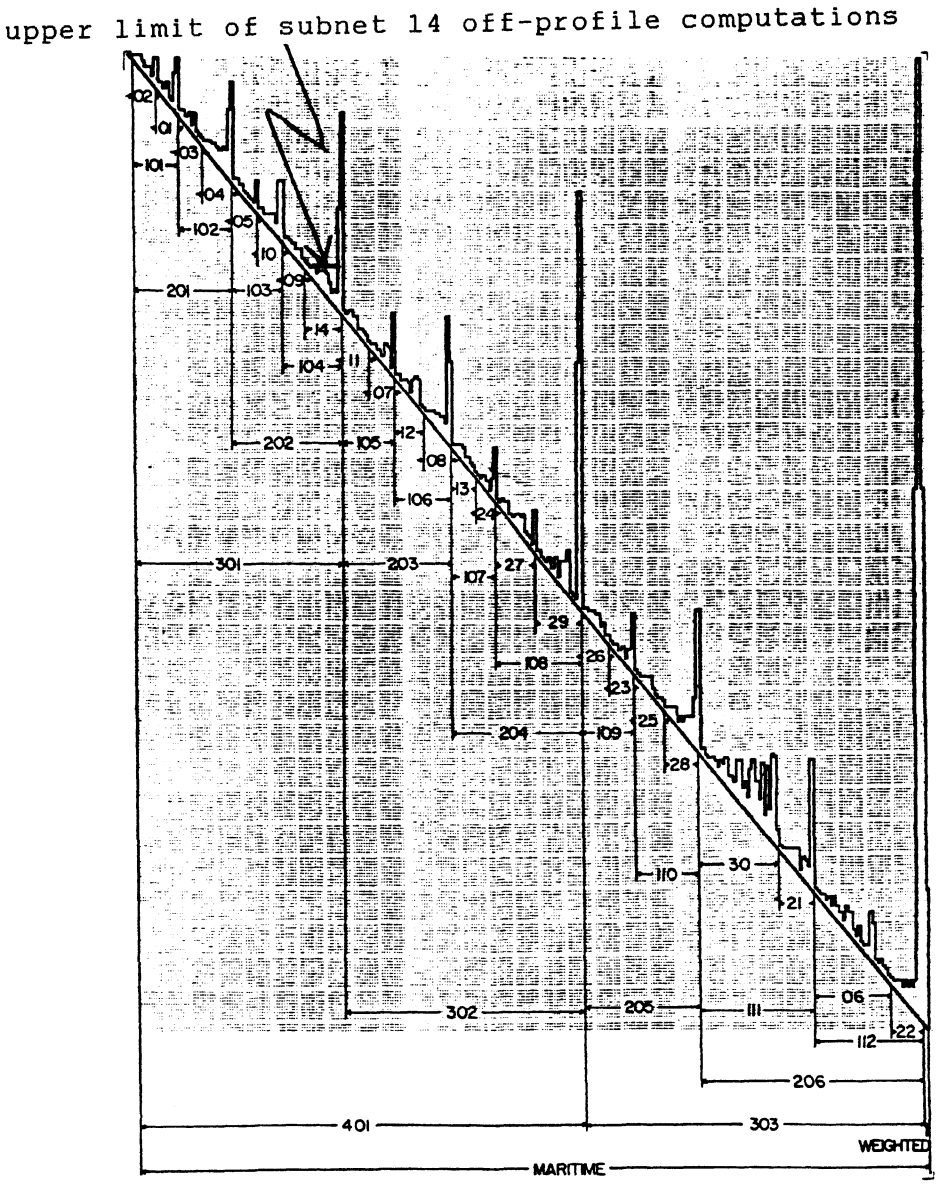

Fig. 7.1 Maritime Inverse Profile (Nickerson, 1981). This shows the profile for which covariances had been computed and therefore available for extraction at very minimal cost. Off-profile elements may be computed at varying cost. The cost escalates the further apart (in the Cholesky factor) the stations are and the further they are from the diagonal.

elements of the covariance matrix, alternative matrices were sought. The alternative covariance matrices should provide results comparable to the rigorous covariance matrix. In order to utilize the inexpensive elements within the profile, the following artificial covariance matrices were proposed and investigated:

(1) Extracted. The covariance submatrix was extracted from the profile. Elements within the profile were obtained readily and inexpensively. Elements outside the profile were assumed to be zero.

(2) Diagonal 2x2. Only the diagonal 2x2 elements of the extracted covariance submatrix were kept. All others were assumed to be zero. This case is suitable for the intra-station weighting that is currently reflected in photogrammetric block adjustment programs UNBASC2, GEBAT, BMAC, PATM-43 and SPACEM.

(3) Estimated. Instead of assuming zero covariances for off-profile elements, they were estimated. The estimation was based on the observation that the covariance matrix was highly patterned (see Figures 5.1 to 5.3). Correlation coefficients of 0.9 for ϕ/ϕ and λ/λ and -0.1 for ϕ/λ were used.

Criterion matrices (Molenaar, 1981) were not considered as the concept requires the original covariance matrix (could be very expensive to compute) to be transformed to an S-base.

7.3.3 Results of Artificial Covariance Matrices

A test densification with actual data (Nickerson, 1982) was performed where results of the three artificial covariance matrices were compared with those obtained with the rigorous covariance matrix (Fig. 5.1 transformed to the plane). Program GEOPAN (Steeves, 1978), a geodetic plane adjustment program, was used as it provided a rigorous input and output of covariance matrices with weighted stations.

In all three cases, the use of the artificial covariances results in differential distortions given by eq. (2.29). Furthermore, the precision of the densification observations was of the same order of magnitude as the weighted stations, resulting in a highly correlated covariance matrix. Results of the test shown in Table 7.1 confirm that the ripple effects were indeed spread thoughout the entire solution vector. A summary of the results for the three cases follows.

(1) Extracted Case. Because of the high correlation of the weighted stations, the zero variances distorted the coordinates significantly. Fig. 7.2 shows the distortion vectors. Most of them were larger than the relative error ellipses of the rigorously weighted case. Three exceeded even the abolute error ellipses. This test showed that the off-profile covariances should not be neglected. Nickerson (1982) also found that the missing elements gave an improper Blaha adjustment - the extracted covariance submatrix was not positive definite.

(2) Diagonal 2x2 Case. The distortions were smaller than those weighted with extracted covariances (see table 7.1). They were all smaller than the absolute error ellipses of the rigorously weighted case, but some were larger than the relative error ellipses (see Fig. 7.2).

(3) Estimated Case. Distortions were the smallest among the three cases (table 7.1). They were smaller than the relative error ellipses. The importance of the off-diagonal and off-profile elements of the apriori covariance matrix is thus confirmed.

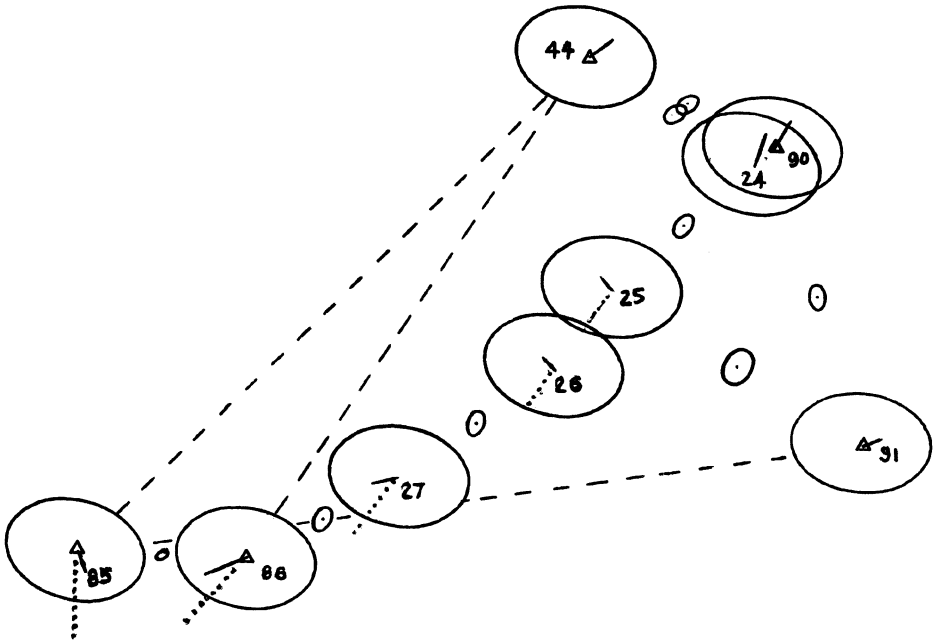

Fig. 7.2 Diagonal & Extracted Versus Rigorous Case. Distortion vectors arising from the use of extracted and diagonal covariances instead of the full covariance submatrix. Absolute and relative error ellipses (Nickerson, 1982) are from the rigorously weighted densification. The vector scale is the same as the ellipse scale.

——— Diagonal minus Weighted.
..... Extracted minus Weighted.
- - - Off-profile covariance. Not in Extracted.
△ Control Points

Scale of points 0 +----------+ 1 km
Scale of ellipses 0 +----------+ 0.1 m
Scale of distortion vectors 0 +----------+ 10 cm

Point	Extracted		Diagonal		Estimated	
24	-0.28	-0.39	0.57	1.65	-0.04	-0.04
25	-1.36	-1.74	-0.28	0.75	0.08	-0.32
26	-1.63	-2.32	-0.54	0.37	0.12	-0.41
27	-2.83	-3.65	-1.51	-0.45	0.05	-0.45
90	-0.14	0.23	0.69	1.75	-0.08	-0.04
91	0.03	-0.15	0.90	0.17	-0.28	-0.27
85	0.06	-5.42	0.64	-1.32	-0.06	0.17
86	-3.98	-4.79	-2.45	-1.1	-0.10	-0.32
44	0.20	-1.19	1.07	1.07	0.50	-0.82

Table 7.1 Coordinate Differences Between Weighting Schemes. Differences (easting, northing) = artificial minus rigorous weights (cm). Observation standard deviations vary from 1.3 to 5.2 arcseconds for directions and from 0.5 to 1.4 cm for distances.

7.4 Statistical Assessment of Integration

The contemporary use of check points to assess the integration of photogrammetric densification is inadequate especially when these points are highly correlated. As the weighted stations approach is gaining popularity in the geodetic community in Canada (see for example Chamberlain et al, 1985 and Steeves & Penton, 1985), photogrammetric densification must try to meet the same guidelines if the approach is to gain favor over the geodetic approach. One of the criteria for acceptance of the integration of the densification network with the existing network is a statistical analysis of the changes in the coordinates of

the weighted stations. The proposed test requires that the covariance matrix of control points before and after the weighted station adjustment be known.

The test of the null hypothesis that $\Delta\hat{x} = 0$, that is $\hat{x}1 = \hat{x}2$, is given by the quadratic form

$$y = (\Delta\hat{x})^T P(\Delta\hat{x}) < \chi^2_{df,1-\alpha} \qquad (7.1)$$

for df degrees of freedom (number of weighted station parameters, in this case) and the desired confidence level $1-\alpha$. Different P matrices have been used. McLaughlin et al (1976) suggested the use of the inverse of either the apriori or aposteriori covaraince matrix, P1 or P2 respectively. A practical problem arises when the use of P1 fails the test but the use of P2 passes, or vice-versa. Thompson et al (1979, pg 126) suggested that either P1 or P2 could be used provided they are of similar precision. The better approach is to use $P\Delta$, the inverse of the covariance matrix of the coordinate differences which is given (Steeves, 1983) by

$$C\Delta = C1 - C2 = (P\Delta)^{-1} \qquad (7.2)$$

For the different weighting schemes, the significance in the coordinate changes of the weighted stations (summerized in Table 7.2) was tested using the three statistics. The results are shown in Table 7.3 along with

their corresponding aposteriori variance factors.

Point	Extracted		Diagonal		Estimated		Weighted	
90	-0.01	-0.01	0.82	1.97	0.06	0.18	0.14	0.22
91	0.03	0.01	0.90	0.33	-0.28	-0.11	-0.00	0.16
85	-0.42	-5.31	0.16	-1.21	-0.54	0.28	-0.48	0.11
86	-4.44	-4.72	-2.91	-1.03	-0.56	-0.25	-0.46	0.08
44	-0.11	-0.89	0.09	-2.08	0.96	0.18	0.39	-1.71

Table 7.2 Coordinate Changes (Easting, Northing in cm) of the Weighted Stations.

y	Extracted	Diagonal	Estimated	Weighted
$P\Delta$	-24.8	-20.6	-2.3	4.6
P1	163.1	112.1	9.04	2.85
P2	52.23	39.7	20.5	11.1
$\hat{\sigma}_0^2$	0.35	0.42	0.57	0.71

Table 7.3 Statistical Assessment of Coordinate Changes in the Weighted Stations. The chi-squared critical value for the 10 degrees of freedom at the 95% confidence level is 18.3. While P1 was not scaled, P2 was scaled by the aposteriori variance factors shown.

All the artificial covariances produced $C\Delta$ that were non-positive definite and thus unsuitable for the test. As shown in Table 7.3, the quadratic forms for the extracted, diagonal and estimated cases were all negative when the matrix $P\Delta$ was used. The problem could be due to either

improper scaling or errors in P1. The latter could be the result of gross errors and errorneous weighting that led to differential distortions of the types shown in equations (2.27a), (2.28a) and (2.29a).

In the rigorously weighted case the test passed for all statistics (P_Δ, P1 and P2) used, but in the extracted and diagonal cases the test failed regardless of the statistics used. In the estimated case, the test passed when the inverse of the apriori covariance matrix (P1) was used but failed when the inverse of the aposteriori covariance matrix (P2) was used.

CHAPTER VIII

CONCLUSIONS AND RECOMMENDATIONS

The distortions due to errors in the bundle adjustment design matrices and the cause and effects of a highly correlated covariance matrix of the ground control points are summarized. Recommendations for further investigations are also presented.

The design matrices of the programs UNBASC2 and GEBAT were revised to account for the additional parameters being a function of the radial distance of the image points. The UNBASC2 revisions resulted in improvements of the adjusted coordinates of up to two micrometres, using the Edmunston test data. Without the revisions in GEBAT, 50 to 100 percent of the intended modelling of the additional parameters was not accounted for. However, the partial

derivatives of the model with respect to the principal point coordinates represented second order effects compared to the harmonic functions themselves. Thus the effects on the adjusted coordinates of the image points did not show much improvement for the test data supplied.

The distortions due to the defects in the design matrices are good candidates for the application of the differential distortion analysis developed in this thesis. However, unless the required matrices can be recovered from within the programs, the analysis may only be limited to estimating orders of magnitude of the distortions or examining patterns.

One evident pattern is seen in the effects of a differential change in the weight matrices of the observables and weighted parameters. While the effects on the solution and residual vectors are small, the effects on their covariance matrices can be quite large.

Thus, although the effects on the image coordinates may only be up to half a micrometre, the small distortions due to the erroneous weights of the ground control points in UNBASC2 could affect the standard deviations of these coordinates by at least a similar magnitude.

The importance of the weights of the ground control points was established. Neglecting high covariances, such as those found in the LRIS ATS77 readjustment, caused concern. Investigations into the causes of these high correlations led to the conclusion that they are the result of the particular densification. As is often the case nowadays, densification observations are becoming more precise. If the precision of the observations is comparable to the precision of the coordinates of the control network to be densified, the resulting covariance matrix is highly correlated.

The inadequacy of the control networks compared to densification precision to yield a highly correlated covariance matrix was also revealed in two other geodetic network adjustments that used different program packages.

The BMAC simulation also showed high correlations when the ground control points for the bundle adjustment were of lower precision than the photogrammetric observations. Depending on the ratio of the precisions of image and ground control point coordinates, this high correlation may extend throughout the entire inverse of the normal equations. In the photogrammetric simulation, the ratio went up to 1000 before the pattern of high

correlation became similar to the ATS77 pattern. Compared with the ATS77 ratio of 10, this seemed to be quite high. Further tests with larger blocks and different photo scales to determine the critical ratio are recommended.

A consequence of a highly correlated covariance matrix is that an error is no longer localized according to the ripple effects. As shown by the differential distortion analysis, the error is spread throughout the entire solution vector.

Due to the highly correlated nature of ground control points, a proper weighting scheme was sought. The inclusion of the inter-station covariances is more important than the intra-station covariances currently implemented in most bundle adjustment programs. Unfortunately, the covariance matrix of ground control points can be very expensive to compute even for the subset required for a typical photogrammetric block. Tests were therefore conducted on alternative covariance matrices: extracted, diagonal and estimated, yielding increasingly better coordinates in that order.

Although these approximate covariance matrices may produce acceptable coordinates, the most rigorous manner to

account for the relative precision of the ground control points is to propagate their full covariance matrix in the bundle adjustment. Further, correct covariance matrices may not otherwise be generated for appropriate statistical interval testing on proper integration.

With the unique opportunity of the availability of the covariance matrix from LRIS, it is recommended that a testblock be established. The test data may be available from recently flown photography over targetted ground control points. Different LRIS projects may offer choices of check point configurations.

By fully propagating the covariance matrix of the ground control points, a rigorous covariance matrix of the densification coordinates may then be obtained. It is recommended that the contemporary estimator of the root mean square error of the check points be compared with the proper statistical interval estimation.

REFERENCES

Ackermann, F. (1981): "Reliability and Gross Error Detection in Photogrammetric Blocks ", Proc. Int. Symposium on Geodetic Networks & Computations, IAG, Munich.

Blais, J.A.R. & M.A. Chapman (1983): "The Use of Relative Terrestrial Control Data in Space-M Photogrammetric Block Adjustments", Seminar paper on SPACE-M Extensions and Conversions, University of Calgary.

Bronson, R. (1970): "Matrix Methods: An Introduction", Academic Press, New York.

Brown D. C. (1974): "Bundle Adjustment with Strip- and Block-Invariant Parameters", Comm III, ISP Symposium, Munich.

Brown, D. C. (1977): "Densification of Urban Geodetic Nets", PE&RS, vol 43, #4, April.

Chapman, M. (1985): Personal Communication, University of Calgary.

Chamberlain, C., R. Steeves, & C. Penton (1985): "A Scenario for the Maintenance of the Canadian Geodetic Network", Geodetic Survey of Canada, Ottawa.

Cramer N., P. Vanicek, Taryydes (1985): "Rigorous Updating of Adjusted Networks", CIS Convention, Edmonton.

Dare, P. & P. Vanicek (1982): "Strength Analysis of Horizontal Networks Using Strain", Paper presented at the meeting of FIG special Study Group 5B (Survey Control Networks), Aalborg, Denmark.

EMR (1978): "Specifications and Recommendations for Control Surveys and Survey Markers", Surveys & Mapping Branch, Ottawa.

El-Hakim (1979): "Potentials and Limitations of Photogrammetry for Precision Surveying", Phd Thesis, Dept of Surveying Engineering, the University of New Brunswick, Fredericton.

El-Hakim (1981): "A Practical Study of Gross-Error Detection in Bundle Adjustment", The Canadian Surveyor, vol 35, #4, December.

El-Hakim (1982): "Results from a Precise Photogrammetric Densification of Urban Control Network", The Canadian Surveyor, vol 36.

Faddeev, D. K. & V. N. Faddeeva, (1963): "Computational Methods of Linear Algebra", W. H. Freeman & Company, San Francisco.

Faig, W. (1973): "Parameters of Interior Orientation and Their Correlations", ASP Fall Convention, Orlando, Florida.

Forstner, W. & R. Schroth (1981): "On the Estimation of Covariance Matrices for Photogrammetric Image Coordinates", Proc. Int. Symposium on Geodetic Networks & Computations, IAG, Munich.

Frazer, R. A. & A. R. Collar (1965): "Elementary Matrices and Some Applications to Dynamics and Differential Equations", Cambridge University Press, Cambridge.

Grun, A. (1978): "Experiences With Self-Calibrating Bundle Adjustment", ASP Convention, March, Washington.

Hamilton, W. C. (1964): "Statistics in Physical Science", the Ronald Press Co., New York.

Hanson, R. A. (1978): "A Posteriori Error Propagation", Proc. 2nd Int. Symposium on Problems Related to the Redefinition of North American Geodetic Networks, NOAA, Arlington.

Hees, G. L. Strang van (1982): "Variance Transformations of Geodetic Networks", manuscripta geodaetica.

Hornik, H. (1981): "The Effect of the Variation of the Design in a Large Network, Shown for Block D of RETRIG", Proc. Int. Symposium on Geodetic Networks & Computations, IAG, Munich.

Hosford, Impley, Welter & Associates Ltd (1983): "ASC Observations: Municipality of Crowsnest Pass, Project 83020 (Framework)", Alberta Bureau of Surveying and Mapping, Edmonton.

Jacobsen, K. (1980): "Bundle Block Adjustment with Small Format Photographs", presented paper, Comm III 14th Congress, ISP, Hamburg.

Jacobsen, K. (1984): "Analysis of Remaining Systematic Image Errors", Comm III, 15th Congress, ISPRS, Rio de Janeiro.

Kipela, E. (1980): "Compensation of Systematic Errors of Image and Model Coordinates", invited paper, Comm III 14th Congress, ISP, Hamburg.

Krakiwsky, E. (1975): "A Synthesis of Recent Advances in the Method of Least Squares", Lecture Notes # 42, Dept. of Surveying Engineering, the University of New Brunswick, Fredericton.

Kupfer, G. & L. Mauelshagen (1980): "Correlations and Standard Errors in Bundle Block Adjustment With Some Emphasis on Additional Parameters", presented paper, Comm III 14th Congress, ISP, Hamburg.

Larsson, R. (1984): "An Efficient Algorithm for the Computation of the Inverse in Bundle Adjustment Systems", Comm III, 15 Congress, ISPRS, Rio de Janeiro.

Ligterink, G. H. (1984): "Aerial Triangulation by Independent Models; the Covariance Matrix of the Observations and Their Influence", Comm III, 15th Congress, ISPRS, Rio de Janeiro.

Lucas, J. R. (1978): "Photogrammetric Control Densification Project", Proc. 2nd Int. Symposium on Problems Related to the Redefinition of North American Geodetic Networks, NOAA, Arlington.

McLaughin et al (1976): "The Maritime Cadastral Accuracy Study", report prepared for LRIS, Dept. of Surveying Engineering, the University of New Brunswick, Fredericton.

Meissl, P. (1978): "A Priori Prediction of Roundoff Error Accumulation During the Adjustment of the United States Ground Control Network by the Helmert Blocking Technique", Proc. 2nd Int. Symposium on Problems Related to the Redefinition of North American Geodetic Networks, NOAA, Arlington.

Meixner, H. (1972): "A Universal Computer Program for Analytical Aerotriangulation", presented paper, Comm III, 12th Congress, ISP, Ottawa.

Milbert, D. G. (1985): "A Note on Observation Decorrelation, Variances of Residuals, and Redundancy Numbers", Bull. Geod. 59.

Molenaar, M. (1981): "S-transformations and Artificial Covariance Matrices in Photogrammetry", ITC Journal 1981-1.

Molenaar, M. (1984): "The Connection of Aerotriangulation Blocks and Ground Control Reconsidered", ITC Journal 1984-1.

Moniwa, H. (1977): "Analytical Photogrammetric System with Self-Calibration and Its Applications", Phd Thesis, Dept. of Surveying Engineering, the University of New Brunswick, Fredericton.

Moniwa, H. (1980): "The Concept of 'Photo-Variant' Self-Calibration and its Application in Block Adjustment with Bundles", presented paper, Comm IV, 14th Congress, ISP, Hamburg.

Nickerson, B. G. (1979): "Horizontal Network Design Using Interactive Computer Graphics", MScE Thesis, Dept. of Surveying Engineering, the University of New Brunswick, Fredericton.

Nickerson, B. G. (1981): "LEAP - LRIS Ellipsoidal Adjustment Package - System Overview", Surveys and Mapping Division, LRIS, Summerside.

Nickerson, B. G. (1982): "Investigations of the Implementation of the Blaha Algorithm for Mapping Plane Adjustment Covariance Propagation", Surveys and Mapping Division, LRIS, Summerside.

Nickerson, B. G. & W. Knight (1983): "LRIS Ellipsoidal Adjustment Package (LEAP) Computational Improvement", Surveys and Mapping Division, LRIS, Summerside.

Rosculet, D. (1980): "Recursive Methods for the Simultaneous Adjustment of Photogrammetric and Geodetic Observations in Analytical Aerotriangulation", presented paper, Comm III 14th Congress, ISP, Hamburg.

Schroth, R. (1984): "An Extended Mathematical Model for Aerial Triangulation", Comm III, 15th Congress, ISPRS, Rio de Janeiro.

Shell Canada Resources Ltd (1978): "Doppler Satellite Survey - Bonnyville, Alberta", report to Alberta Transportation, (Alberta Bureau of Surveying and Mapping), Edmonton.

Steeves, R. (1978): "A User's Manual For Program GEOPAN Geodetic plane Adjustment and Analysis", Technical Report #54, Dept. of Surveying Engineering, the University of New Brunswick, Fredericton.

Steeves, R. (1983): "Statistical Analysis of Control Coordinate Changes Resulting From The Integration of Geodetic Networks", Geodetic Survey of Canada, Ottawa.

Steeves, R. & C. Penton (1985): "Guidelines for the Integration of Geodetic Networks in Canada", Geodetic Survey of Canada, Ottawa.

Thomson, D. B., E. J. Krakiwsky & B. G. Nickerson (1979): "A Manual for the Establishment and Assessment of Horizontal Survey Networks in the Maritime Provinces", Technical Report #52, Dept. of Surveying Engineering, the University of New Brunswick, Fredericton.

Vanicek, P. & E. Krakiwsky (1982): "Geodesy the Concepts", North Holland, Amsterdam.

Voon, A. J. P. N. (1984): "Classification of Control Stations", paper presented to Victoria meeting of CCSM Secondary Integration Subcommittee, Surveys and Mapping Division, LRIS, Summerside.

Voorden, A. van (1984): "Testing and Internal Reliability in the Process of Analytical Absolute Orientation", Comm III, 15th Congress, ISPRS, Rio de Janeiro.

Wells, D. E. (1971): "Matrices", Lecture Notes #15, Dept. of Surveying Engineering, the University of New Brunswick, Fredericton.